Graduate Student Theses, Dissertations, & Professional Papers

Graduate School

2018

Evaluation of Autonomously Measured Alkalinity, pH, and pCO2 Variability on a Coral Reef

Brittany Peterson

Let us know how access to this document benefits you.

Follow this and additional works at: https://scholarworks.umt.edu/etd

Part of the Analytical Chemistry Commons, and the Environmental Chemistry Commons

EVALUATION OF AUTONOMOUSLY MEASURED ALKALINITY, pH, AND $p\mathrm{CO}_2$

VARIABILITY ON A CORAL REEF

By

BRITTANY PETERSON

B.A. Chemistry, Whitman College, Walla Walla, Washington, 2008

Thesis

presented in partial fulfillment of the requirements
for the degree of

Master of Science
in Chemistry, Environmental/Analytical

The University of Montana
Missoula, MT

December 2018

Approved by:

Scott Whittenburg, Dean of The Graduate School
Graduate School

Dr. Michael D. DeGrandpre, Chair
Chemistry

Dr. Christopher Palmer
Chemistry

Dr. Maury Valett
Biological Sciences

Evaluation of Autonomously Measured Alkalinity, pH, and pCO$_2$ Variability on a Coral Reef

Chairperson: Mike DeGrandpre

Currently, our understanding of alkalinity (A$_T$) variability in highly dynamic environments such as coral reefs is limited by the dearth of A$_T$ measurements. In order to better characterize these environments, high temporal resolution A$_T$ data are needed. This work employed the newly developed Submersible Autonomous Moored Instrument for Alkalinity (SAMI-alk), a fully autonomous in situ A$_T$ analyzer, to study seawater A$_T$ variability. The main goals of this research were to evaluate the utility of combining the SAMI-alk data with currently available in situ measurements of pH and partial pressure of carbon dioxide (pCO$_2$) to characterize the inorganic carbon cycle, and to measure A$_T$ variability and determine what drives it on a coral reef.

Autonomous A$_T$ and pH sensors (SAMI-alk and SAMI-pH) were deployed along with existing pCO$_2$ (MAPCO2) and pH (SeaFET) sensors in Kanoehe Bay, HI from June 4 – 21, 2013. The results show that the pH – A$_T$ combination can provide important information about autonomously measured in situ data quality, and that it can be used to fully characterize the inorganic CO$_2$ system in seawater. The SAMI-alk data were also used to examine A$_T$ variability and thereby calcification rates on coral reefs in Kaneohe Bay. A$_T$ varied by more than 100 μmol kg^{-1} on a diel basis due to CaCO$_3$ production and dissolution. Dissolved inorganic carbon (DIC), calculated from the pH – A$_T$ sensor pair, varied by more than 200 μmol kg^{-1}, due primarily to biological metabolism on the reef. Reef calcification and metabolism dramatically alter the seawater chemistry from the open ocean source water and drive the large diel changes in all measured inorganic carbon parameters (*i.e.* aragonite saturation state (Ω$_{arag}$), pH, pCO$_2$, A$_T$, DIC). This data set demonstrates the value of a high-quality in situ A$_T$ analyzer in a coral reef environment; making it possible to determine combined CO$_2$ system variability with unprecedented temporal resolution. These data show that NEC can be consistently sustained (net CaCO$_3$ production) until a threshold level of net respiration (NEP) is reached, around -50 (mmol m^{-2} h^{-1}), which corresponds to an A$_T$: DIC ratio of about 1:1.

Acknowledgements

Table of Contents

List of Figures

List of Tables

.

CHAPTER 1

Introduction

1.1 Overview

The level of carbon dioxide (CO_2) in the atmosphere has increased from 280 to ~400 µatm due to fossil fuel consumption since the start of the industrial revolution (Takahashi et al., 2009; Bates et al., 2014; Sutton et al., 2014) (Fig. 1.1). The oceans have mitigated an even greater increase in atmospheric pCO_2 by absorbing about 25% of the anthropogenic CO_2 in the atmosphere (Sabine et al., 2004). This uptake of CO_2 has decreased pH by ~0.13 pH units changing the inorganic carbon concentration and speciation (Broecker et al., 1979; Caldeira and Wickett, 2003; Dore et al., 2009). The decrease in pH is called 'ocean acidification' (Raven et al., 2005; Hönisch et al., 2012) (Fig. 1.1). Ocean acidification changes seawater chemistry speciation, for example converting carbonate (CO_3^{2-}) to bicarbonate (HCO_3^-), which can negatively affect marine ecosystems. Anthropogenic ocean acidification could contribute to a cascade of events that harm various ecological mechanisms such as shell building on coral reefs (Kleypas et al., 2006) and including services relied upon directly by humankind (Raven et al., 2005). The potential impacts of ocean acidification are far reaching, but their full extent is unknown.

CO$_2$ Time Series in the North Pacific

Legend:
- Mauna Loa Atmospheric CO$_2$ (ppm)
- Aloha seawater pCO$_2$ insitu (µatm)
- Aloha seawater pH (insitu)

NOAA PMEL Carbon Program: www.pmel.noaa.gov/co2/
Mauna Loa data from NOAA ESRL
ALOHA data adapted from Dore et al. 2009
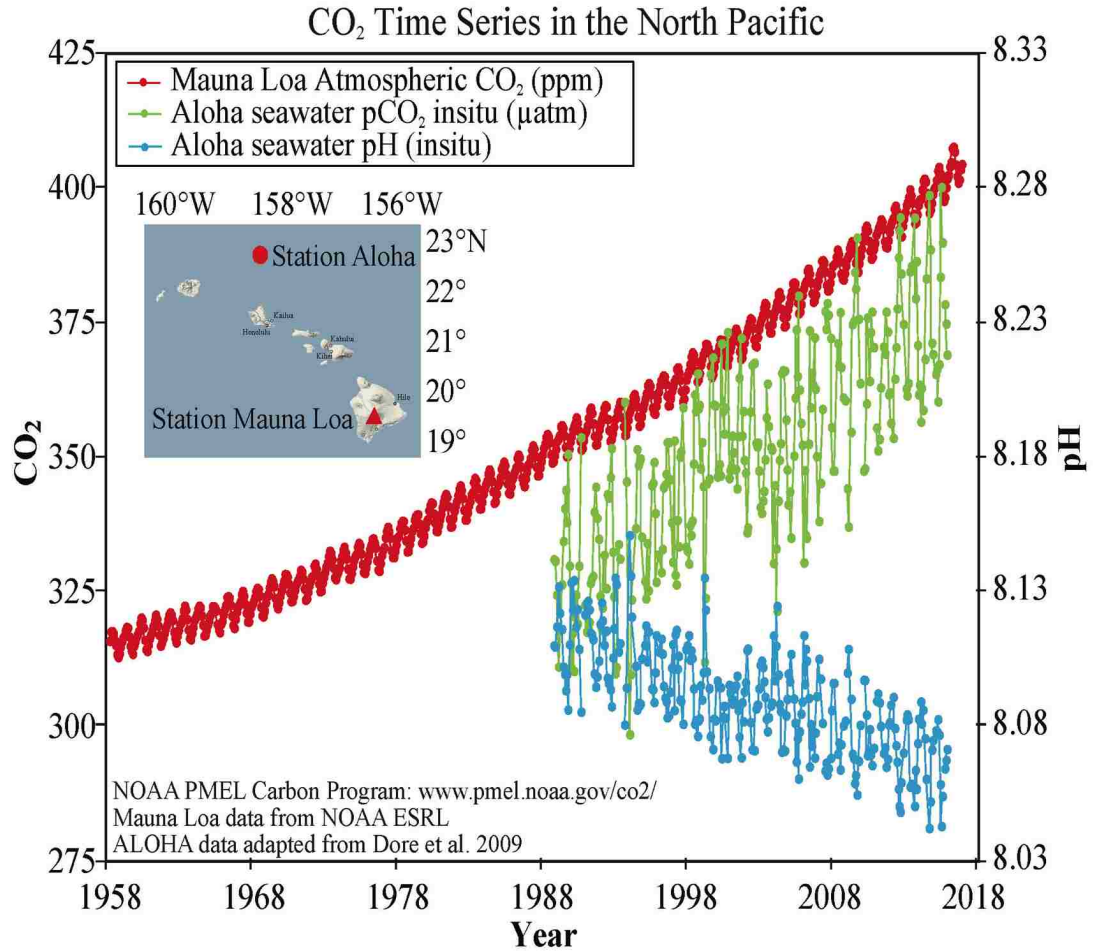
Data: Mauna Loa (ftp://aftp.cmdl.noaa.gov/products/trends/co2/co2_mm_mlo.txt) ALOHA (http://hahana.soest.hawaii.edu/hot/products/HOT_surface_CO2.txt)
Ref: J.E. Dore et al, 2009. Physical and biogeochemical modulation of ocean acidification in the central North Pacific. *Proc Natl Acad Sci USA* **106**:12235-12240.

Figure 1:1 Decades long trends in atmospheric (red) and surface seawater pCO$_2$ (green), and pH (blue), from the Hawaii Ocean Time-series (HOT) station ALOHA (the Mona Loa Observatory Hawaii (atmospheric pCO$_2$). Photosynthetic activity causes seasonal CO$_2$ swings particularly in the northern hemisphere where CO$_2$ is consumed in the summer and produced in the winter. Figure from the NOAA PMEL Carbon Program.

The carbonate equilibria are presented below in Eqns. (1.1 – 1.5). When CO$_2$ dissolves in water (Eqn. 1.1) it forms carbonic acid (H$_2$CO$_3$) (Eqn. 1.2). It is difficult to experimentally distinguish between CO$_2$ (aq) and H$_2$CO$_3$ so they are combined into one theoretical species (H$_2$CO$_3^*$) (Eqn. 1.3). The net result of CO$_2$ dissolved in water is an increase in hydrogen ions, hence the term 'ocean acidification' (Eqn. 1.4).

$$CO_2 \text{ (g)} \leftrightarrow CO_2 \text{ (aq)} \tag{1.1}$$

$$CO_2 \text{ (aq)} + H_2O \leftrightarrow H_2CO_3 \tag{1.2}$$

$$H_2CO_3{}^* = CO_2 \text{ (aq)} + H_2CO_3 \tag{1.3}$$

$$H_2CO_3{}^* \leftrightarrow H^+ + HCO_3{}^- \tag{1.4}$$

$$HCO_3{}^- \leftrightarrow H^+ + CO_3{}^{2-} \tag{1.5}$$
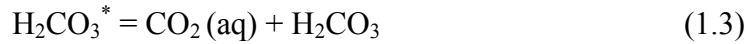
The concentrations of the individual species of the CO_2 system in solution cannot all readily be measured directly. Instead, there are four parameters that can be measured: pH, pCO_2, dissolved inorganic carbon (DIC), and total alkalinity (A_T). The expressions for each parameter are shown in equations 1.5-1.8, where K_H is the Henry's law constant. These are used together to obtain a complete description of the CO_2 system in seawater (Clayton et al., 1995; Lee and Millero, 1995; McElligott et al., 1998; Byrne et al., 1999; Lee et al., 2000).

$$pH = -\log[H^+] \tag{1.5}$$

$$pCO_2 = [H_2CO_3{}^*] / K_H \tag{1.6}$$

$$DIC = [H_2CO_3{}^*] + [HCO_3{}^-] + [CO_3{}^{2-}] \tag{1.7}$$

$$A_T = [HCO_3{}^-] + 2[CO_3{}^{2-}] + [B(OH)_4{}^-] + [OH^-] - [H^+] - [HF] - [HSO_4{}^-]$$
$$+ \text{ minor nutrient species} \tag{1.8}$$

Each parameter on the left side (pH, pCO$_2$, DIC and A$_T$) is a commonly

measured inorganic carbon parameter (Dickson et al., 2007). pH (Eqn. 1.5) is measured

either spectrophotometrically or with an ion selective electrode. pCO$_2$ is measured by

equilibrating a sample with a small head space and analyzing it with an infrared (IR)

analyzer (Eqn. 1.6) or using a membrane with enclosed pH indicator (DeGrandpre et al.,

1995). To determine DIC (Eqn. 1.7), a sample is acidified and the CO$_2$ gas that is

produced is extracted and measured coulometrically. Alkalinity (A$_T$), defined as the

number of moles of H$^+$ equivalent to the excess proton acceptors over proton donors,

(Eqn. 1.8) is measured by a titration with hydrochloric acid (HCl). All of the inorganic

carbon species can be calculated with any two of these parameters (Lee and Millero,

1995), but the combined resulting errors in calculating the CO$_2$ system are smallest when

either pH or pCO$_2$ are combined with either DIC or A$_T$ (Clayton et al., 1995; Lee and

Millero, 1995; McElligott et al., 1998; Byrne et al., 1999; Lee et al., 2000; Cullison Gray

et al., 2011).

The DeGrandpre Lab at the University of Montana focuses on the measurement of

these parameters using autonomous sensors. There are commercially available

autonomous instruments available to measure pH and pCO$_2$ (DeGrandpre et al., 1995;

Martz et al., 2003, 2010; Seidel et al., 2008; Sutton et al., 2015). While some progress has

been made toward autonomous systems for measuring A$_T$ and DIC (Watanabe et al.,

2004; Bandstra et al., 2006; Gray et al., 2008; Sayles and Eck, 2009; Li et al., 2013;

Spaulding et al., 2014), there are no commercial instruments available and, prior to this

work, A$_T$ and DIC were limited to lab-based methods, which require automated or

manual sample collection and manual analysis.

Overview *In situ* A_T

Conventional A_T measurements require potentiometric pH and accurate volumetric or gravimetric measurement of the sample and HCl titrant (Hansson and Jagner, 1973; Dickson, 1981). This process is time consuming and requires that samples be collected in the field, transported to the lab for analysis, and manually loaded into the titration cell. In some marine ecosystems, such as coral reefs, the CO_2 system (including A_T) changes rapidly throughout the day (Cai et al., 2010), so in order to measure the full daily (i.e. diel) cycle many samples must be collected at multiple times of the day and night. This makes the task of characterizing short-term A_T variability nearly impossible. Continuous *in situ* A_T measurements are especially important on coral reefs because they can be used to directly quantify ecosystem calcification (Smith and Key, 1975), a key parameter reflecting reef health. As part of this project, the DeGrandpre lab, in collaboration with Sunburst Sensors (Missoula, MT), developed an autonomous A_T system, the Submersible Autonomous Moored Sensor for Alkalinity (SAMI-alk). With this sensor, we now have the ability to measure A_T with unprecedented temporal resolution, and therefore more effectively study coral reefs.

1.2 Coral reefs

The decline in ocean pH since pre-industrial times is accompanied by a decrease in the concentration of carbonate ions (CO_3^{2-}) (Andersson et al., 2005; Orr et al., 2005). The

drop in CO_3^{2-} results in a decreased saturation state for calcium carbonate ($CaCO_3$), which makes it more difficult for many calcifying organisms to produce shells (Gattuso et al., 1999; Raven et al., 2005; Kleypas et al., 2006; Fabry et al., 2008; Doney et al., 2009). While anthropogenic CO_2 dissolves in the oceans, organisms in the water are forming their shells from $CaCO_3$ (Eqns. 1.9 - 10). Aragonite is the key $CaCO_3$ mineral organisms use to produce shell and skeleton material. The saturation state of aragonite is defined in Eqn. 1.9 where Ω_{arag} is the saturation state for aragonite and K_{sp} is the solubility product for aragonite. Lower pH waters are corrosive to aragonite because of the reduced availability of $[CO_3^{2-}]$. The net reaction of increased CO_2 dissolving in seawater also leads to an excess of H^+ (Eqns. 1.3-1.4) against which calcifiers must contend (Hofmann et al., 2010; Jury et al., 2010). Quantifying ecosystem calcification is an important step in understanding coral reef health and then making predictions about the susceptibility of coral reefs to ocean acidification (Langdon et al., 2000; Doney et al., 2009; Andersson and Gledhill, 2013; Shaw et al., 2015). Specific contemporary research questions regarding corals will be discussed in Chapter 4.

$$\Omega_{arag} = \frac{[Ca^{2+}][CO_3^{2-}]}{K_{sp}} \tag{1.9}$$

$$Ca^{2+} + HCO_3^- \leftrightarrow CaCO_3 + H^+ \tag{1.10}$$

1.3 Objectives

The goals of this research are to utilize novel high temporal resolution A_T data to fully characterize A_T in order to better understand CO_2 dynamics in a coral reef

ecosystem. We deployed a SAMI-alk along with a suite of other sensors including a Submersible Autonomous Moored Instrument for pH (SAMI-pH) in Kaneohe Bay, HI in 2013. The SAMI-alk analyzed A_T hourly for 17 days collecting a total of 263 *in situ* measurements capturing multiple diel cycles of A_T and DIC in order to determine calcification and production on the reef (Spaulding et al., 2014). To our knowledge, this is the longest continuous study of A_T variability that has ever been conducted with this temporal resolution. The performance of SAMI-alk during this deployment was evaluated by Spaulding et al. (2014); however, these data were not interpreted in the context of coral reef ecology. Here we present: the 17-day time series of nearly continuous A_T, pH, and pCO$_2$ measurements. Furthermore, this is the first time that 3 CO$_2$ system parameters have been collected together on a mooring. The evaluation will include:

Chapter 2: Experimental design and methods.

Chapter 3: Analysis and characterization of the CO$_2$ system, calculated multiple ways, and a performance evaluation of four autonomous sensors that measure CO$_2$ system parameters.

Chapter 4: Interpretation of the observed variability of calcification and production on the reef, to address the drivers of ecosystem calcification. Specifically, how does the reef biogeochemistry alter the open ocean source water? What controls the relationship between coral productivity (NEC) and inorganic carbon species such as H^+, CO_3^{2-}, and Ω_{arag}? And is there a baseline relationship between CO$_2$ system speciation and NEC that is necessary to maintain current rates of calcification?

Chapter 5: Conclusions and future work.

CHAPTER 2

Methods

2.1 Kaneohe Bay

Kaneohe Bay is located on the eastern side of Oahu, HI (Fig. 2.1). In the bay there is a large barrier coral reef, patch reefs and fringing reefs. The reef is approximately 2.4 km wide, and the bay is 4.3 km wide and 12.7 km long (Shamberger et al., 2011). The bay has eleven freshwater stream inputs and the surrounding watershed is affected by anthropogenic activities such as urban development (De Carlo et al., 2004, 2007; Ringuet and Mackenzie, 2005; Hoover and MacKenzie, 2009). The prevailing wind direction is from the northeast (Smith et al., 1981). A circulation model of the bay demonstrates that currents are predominately wave-driven (Lowe et al., 2009b, 2009a). The water residence time in Kaneohe Bay varies from hours to more than a month (Lowe et al., 2009b) depending upon wind speed, wave height and the semidiurnal tides, all of which control circulation in the bay. The water at the site is well mixed vertically and horizontally by the northeast trade winds (Smith et al., 1981).
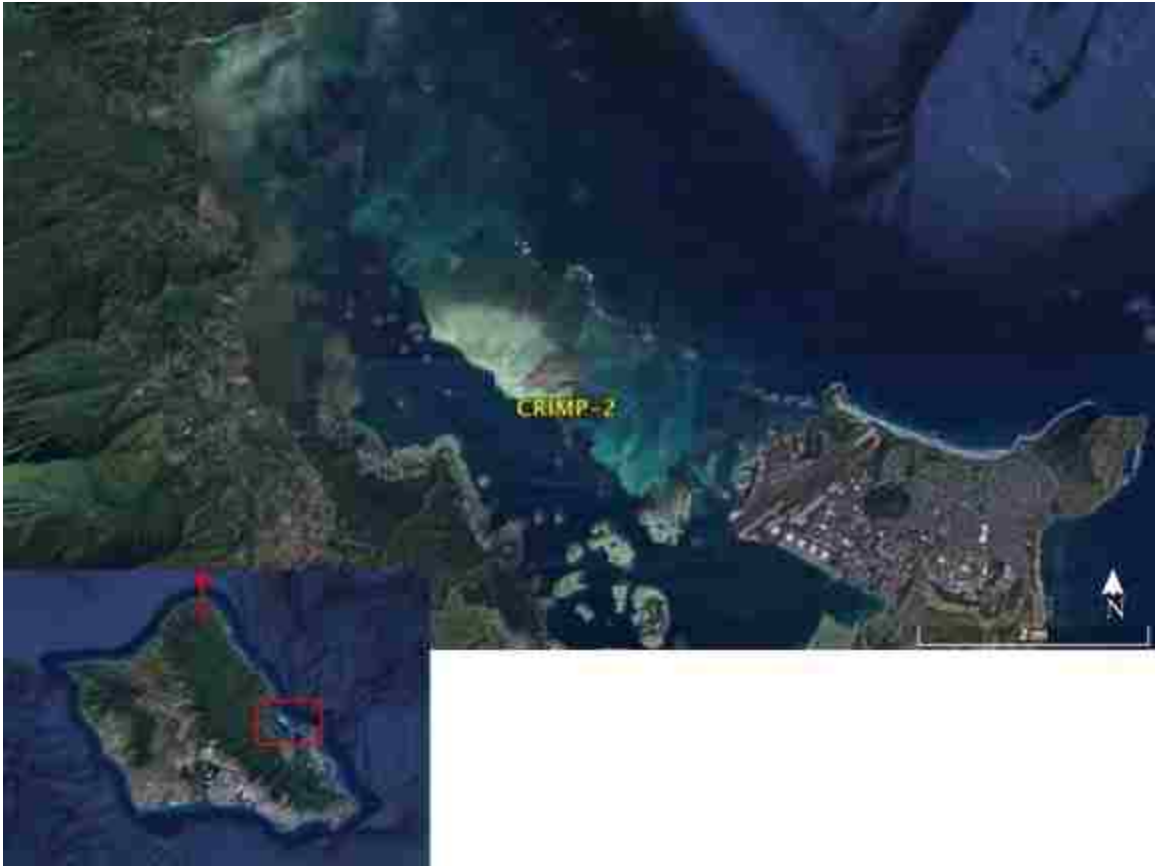
Figure 2:1 Kaneohe Bay, located on the northeast coast of Oahu. SAMI-alk, SAMI-pH, SeaFET and MAPCO2 systems (see text for explanations) were deployed at the CRIMP-2 instrument platform. The red arrow indicates north and the direction of the Hawaiian Ocean Time-series (HOT) station ALOHA.

The SAMI-alk was deployed in Kaneohe Bay because there are large daily diurnal A_T swings in the Bay caused by $CaCO_3$ formation and dissolution on the reef (Shamberger et al., 2011). There is an existing instrument platform, the Coral Reef Instrumented Monitoring and CO_2-Platform (CRIMP-2), on which sensors that measure the pCO_2, temperature, and salinity were already deployed (21.46 °N, 157.80 °W) (Shamberger et al., 2011; Drupp et al., 2013). CRIMP-2 sits in approximately 3 m of water over sandy sediment on the inside edge of the barrier reef (Fig. 2.1). Water flow at the buoy is unidirectional from the open ocean over the reef (Lowe et al., 2009b, 2009a); water then

exits the bay through one of two channels, a deep shipping channel in the northern bay, or the Sampan Channel in the central bay (Lowe et al., 2009b, 2009a). We deployed the SAMI-alk at the CRIMP-2 (Fig. 2.2) buoy along with a SAMI-pH (Seidel et al., 2008), an existing MAPCO2 system (Sutton et al., 2015), a SeaFET pH sensor (Martz et al., 2010), and a Seabird CTD which measures salinity, temperature, and depth (Spaulding et al., 2014). Regrettably, no O_2 sensors were deployed. The water chemistry at CRIMP-2 is representative of the overall water chemistry on the reef (Drupp et al., 2013).

Figure 2:2 Divers at the CRIPM-2 buoy in Kaneohe Bay during the June 2013 SAMI-alk deployment. The MAPCO$_2$ system is housed inside the yellow buoy. The SAMI-alk was suspended below the buoy, see Figure 2.4.

2.2 *In situ* data: instruments and measurements

2.2.1 A_T measured by Tracer Monitored Titration

As stated in Chapter 1, conventional A_T titrations necessitate accurate volumetric or gravimetric measurements of both sample and titrant (Hansson and Jagner, 1973; Dickson, 1992). Spectrophotometric pH measurements have improved the accuracy of the titration (Breland and Byrne, 1993; Yao and Byrne, 1998). The tracer-monitored titration (TMT), based on a spectrophotometric method, uses a spectrophotometric indicator in the titrant to quantify a dilution factor for the titrant and sample (Martz et al., 2006). This removes the necessity of having accurate volumetric or gravimetric measurements (DeGrandpre et al., 2011). The SAMI-alk uses the TMT method to measure A_T autonomously in situ.
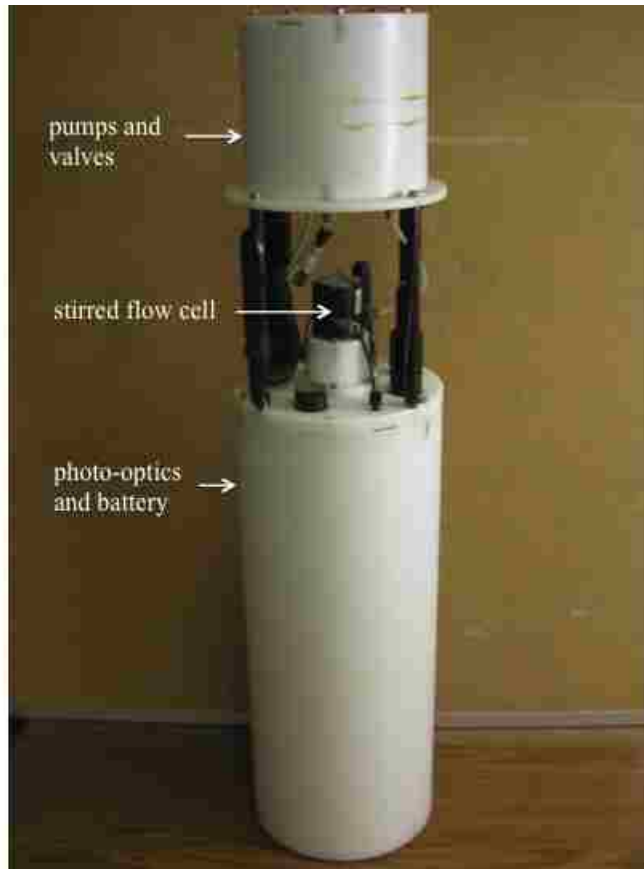
Figure 2:3 The prototype of the Submersible Autonomous Moored Instrument for alkalinity (SAMI-alk) deployed in this study (Spaulding et al., 2014).

Spaulding et al., (2014) evaluated the performance of a prototype instrument built in the DeGrandpre lab, the SAMI-alk, using the TMT methodology (Fig. 2.3). The first *in situ* deployment of the SAMI-alk was done at the Hatfield Marine Sciences Center in Newport, Oregon by Spaulding et al., (2014) in January 2013. It was installed in a 100-gallon tank of continuously flowing Yaquina Bay seawater. The SAMI-alk made hourly measurements for 10 days, and was evaluated using discrete samples taken from the tank with an accuracy and precision of -2.9 ± 6.4 μmol kg^{-1} (n = 33).

For its second in situ evaluation, the SAMI-alk was deployed in Kaneohe Bay, HI. The SAMI-alk was deployed with a 5-μm filter on the inlet to reduce the introduction of

particles into the stirred flow cell, and was secured in a crate suspended directly below

the CRIMP-2 platform (Fig. 2.4) from June 4 – June 20, 2013. The SAMI-alk analyzed

A_T hourly, and measured two sequential A_T standards each day (Spaulding et al., 2014).
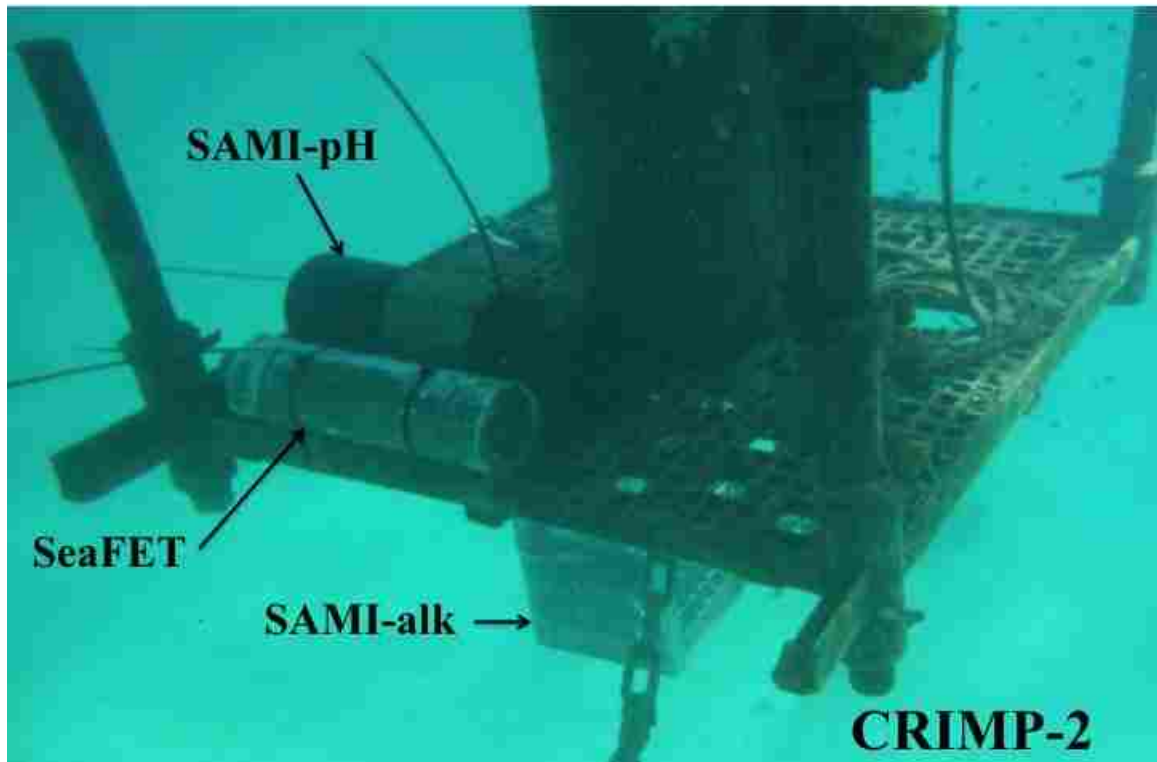
Figure 2:4 Instruments deployed on the CRIMP-2 platform. The MAPCO2 system is above water; only the equilibrator is submerged (not shown). The SAMI-pH, SeaFET, Seabird SBE37-SMP (on opposite side not shown) were attached on the platform, and the SAMI-alk was suspended directly below the platform. The inlet of the SAMI-alk was ~0.5 m below the instruments on the platform.

Because this data set was previously published (Spaulding et al., 2014) it is

included here, rather than in the results section of Chapter 3. The SAMI-alk made 310

seawater A_T measurements (Fig. 2.5) from June 4 – June 20 and an additional 30

measurements on A_T standards. The standards were used to apply a calibration factor to

the SAMI-alk that was adjusted by ~3% over the course of the deployment (Spaulding et

al., 2014). This adjustment was likely necessary due to small changes in the acid

concentration, de-gassing of the reagent in the warm ocean temperatures, and biological

activity inside the reagent bag altering the chemistry as discussed in Spaulding et al.,

(2014). A blank filter, discussed in Spaulding et al., (2014), based on the change in blank

ratio from one titration to the next and discarding titrations with >0.4% change in the

blank ratio, was applied to the raw A_T data reducing the number of A_T measurements

used in this study to 263 samples.
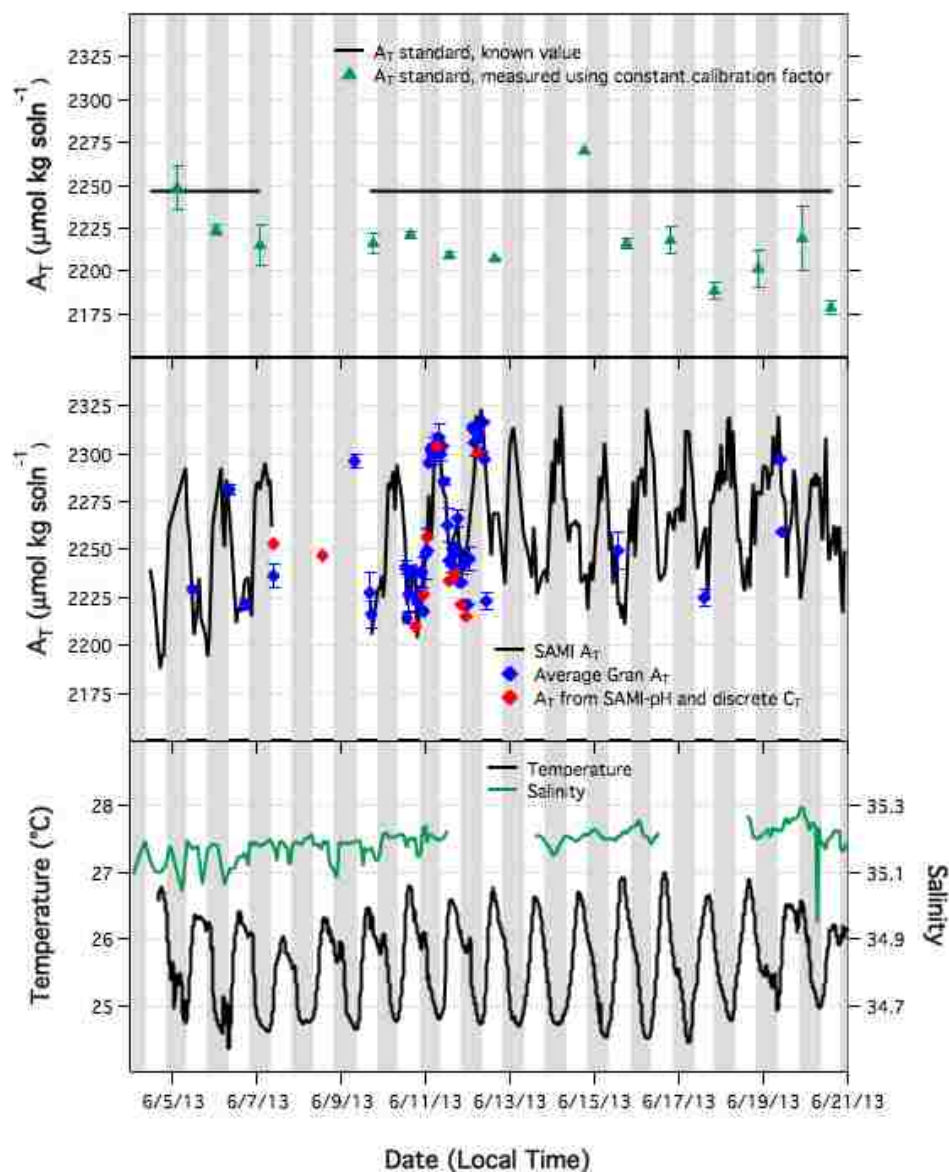
Figure 2:5 Data from CRIMP-2 during the SAMI-alk deployment. Top: A_T measured by the SAMI-alk on an A_T standard. Middle: A_T measured by the SAMI-alk (black line), discrete A_T samples (blue dots), and A_T calculated from the SAMI-pH and discrete DIC samples (red dots) taken over the 17-day time series. Bottom: temperature and salinity. Gray bars represent nighttime. Figure from Spaulding et al., 2014. The gap in data resulted from an error when re-starting the SAMI-alk after downloading data.

The accuracy and precision of the SAMI-alk during the study was -1.6 ± 15.7

μmol kg soln^{-1} based on the difference of the SAMI-alk measurements with the adjusted

standard and blank filtered data, and the discrete A_T samples. The increased blank noise (a blank filter of >0.2% was used in the lab tests), possible build up of small particles in the flow cell, and imperfect timing of the discrete sample collection in an environment where A_T was rapidly changing contributed to the decreased precision of the SAMI-alk compared to lab tests of the sensor. The two days of missing A_T data (Fig. 2.5) are from a software error that occurred while downloading the data. Alkalinity variability on the reef is due almost entirely to diel cycles of calcification, where benthic calcifiers decrease A_T during the day as $CaCO_3$ is formed, and increase A_T at night when rates of $CaCO_3$ formation slows and dissolution occurs (Andersson et al., 2009; Eyre et al., 2014; Albright et al., 2015). Because A_T variability directly reflects calcification rates it is critical to measure the full A_T cycle of coral reefs (Ohde and Woesik, 1999; Bates et al., 2010; Gray et al., 2012; Shaw et al., 2012). A primary goal of this thesis is to interpret this novel data set.

2.2.2 pH: SAMI-pH and SeaFET

The SAMI-pH (Fig. 2.4) executed pH measurements every 10 minutes throughout the deployment. The accuracy of the SAMI-pH is ± 0.003 pH units with a precision of ± 0.001 based on laboratory analysis (Seidel et al., 2008). It employs a spectrophotometric pH measurement described in Seidel et al., (2008). The SeaFET employs an ion-sensitive field effect transistor (ISFET) to make potentiometric pH measurements (Martz et al., 2010). It sampled every three hours until June 10 and then hourly until 1200 hrs on June 16, when the sensor fouled due to a calcium carbonate deposit accumulating on the

ISFET chip. The accuracy of the SeaFET is estimated as ± 0.05 pH units with a precision of ± 0.005 based on laboratory analysis (Martz et al., 2010).

The SAMI-pH was set to sample every 10 minutes, ensuring that we have temporally meaningful points with which to compare each SAMI-alk value. Additionally, it confirms that hourly temporal resolution captures the full range of the carbonate chemistry. The SeaFET pH sensor was deployed at the CRIMP-2 site two months before the SAMI-alk and SAMI-pH. The SeaFET measured pH every three hours until June 10, and then hourly for the rest of its deployment. Its period of data collection overlapped with that of the SAMI-alk and SAMI-pH by 12 days before it became clear that biofouling was affecting the SeaFET pH measurements.

2.2.3 MAPCO$_2$

The MAPCO$_2$ system (Fig. 2.2) uses a LICOR-820 infrared analyzer to measure atmospheric CO$_2$ (pCO$_{2air}$) and sea surface pCO$_2$ (Sutton et al., 2015) from an in situ air-water equilibrator. It recorded data every three hours until June 10 when it was switched to hourly measurements. The data was transmitted daily via Iridium satellite to NOAA/PMEL and were posted at www.pmel.noaa.gov/co2. The MAPCO$_2$ system self calibrates with a zero CO$_2$ gas and a high CO$_2$ gas each measurement, and each measurement takes ~20 minutes with pCO$_2$ recording 17 minutes after the sample is taken and CO$_{2air}$ recorded right after pCO$_2$. The accuracy of the CO$_2$ measurements is conservatively estimated to be within 2.5% of the measured value (Sutton et al., 2015). More details on the scheme of this system can be found in Shamberger et al., (2011), Massaro et al., (2012), and Sutton et al., (2015).

2.2.4 Temperature and Salinity

The SAMI-alk, SAMI-pH, and SeaFET all recorded temperature with integrated thermistors. Additionally, a Sea-Bird conductivity temperature depth sensor (SBE37-SMP) was mounted on the CRIMP-2 platform and recorded temperature and salinity hourly during the study (Fig. 2.5). The MAPCO2 system also makes an oxygen measurement as percent oxygen of the surface seawater divided by percent oxygen of the atmosphere at 4 feet above the water surface (% O_2); the measurements are made in the equilibrated air. However, the oxygen does not come to complete equilibrium, and the rapidly changing oxygen due to biological activity is not captured (Sutton et al., 2015). Sutton et al. (2015) recommends that these O_2 data not be used as quantitative measurements and were not used in this study.

2.3 Discrete samples

Discrete samples were taken throughout the deployment during different times of the day in order to capture the full diel range of CO_2 chemistry on the reef and for data quality control (QC). Samples were taken more intensively (hourly) from June 10 – 12. Samples were collected in 300-mL borosilicate bottles and were fixed with 200 μL of saturated $HgCl_2$ to prevent biological activity from altering water chemistry.

A_T samples (n=59) were analyzed in a local lab by open-cell potentiometric titration (Dickson et al., 2007). Seawater certified reference materials (CRMs) analyzed daily determined an accuracy and precision of -0.4 ± 4.7 μmol kg soln^{-1} for the bench top CRM measurements (n = 44) (Spaulding et al., 2014). The field samples were analyzed in

duplicate with a precision of ± 4 μmol kg soln^{-1}. Discrete samples taken during June 10 –

12 were also analyzed for DIC by coulometric titration (n = 9) (Johnson and Sieburth,

1987; DOE, 1992). The accuracy of the DIC, also established with CRMs, was ~1 $\pm$ 2

μmol kg soln^{-1}.

2.4 Physical parameters

Data for wind (m s^{-1}), tides (m), and light (photosynthetically active radiation,

PAR) (μEinsteins m^{-2} s^{-1}) from the Hawaii Institute of Marine Biology (HIMB) weather

station on Coconut Island in Kaneohe Bay were used for this analysis. Wave height data

were obtained from the Coastal Data Information Program (CDIP) buoy 098 located 6

km southwest of Mokapu Point (~21.414 °N, 157.679 °W).

2.5 Data Analysis

2.5.1 Carbon system calculations

As discussed above, the CO_2 system in seawater can be fully calculated with two

of the measurable parameters. In this study, we fully characterize the seawater CO_2

system of Kaneohe Bay four ways: (1) with SAMI-alk and SAMI-pH, (2) with SAMI-alk

and SeaFET pH, (3) with SAMI-alk and MAPCO$_2$, and (4) SAMI-pH – MAPCO$_2$. Each

set of calculations used the same temperature and salinity data. All calculations were

made using the carbonate equilibrium program CO2SYS (Lewis and Wallace, 1998). The

equilibrium constants used in these calculations were determined by Mehrbach et al.

(1973) refitted by Dickson & Millero (1987). pH on the total hydrogen ion scale was used

with the sulfate constant determined by Dickson et al. (1990). Based on the observed

19

alkalinity changes, associated changes in calcium concentration are not significant relative to the overall calcium concentration. Accordingly, the conservative-salinity based estimate was used for calcium concentration in saturation state (Ω_{arag}) calculations. The results from each pair of measured parameters are analyzed and compared in the following chapter.

The third measurable parameter of the seawater CO_2 system, DIC, was calculated four ways: with the A_T + SAMI-pH, A_T + SeaFET, A_T + pCO_2, and SAMI-pH + pCO_2 in CO2SYS (Lewis and Wallace, 1998). The SAMI-pH + A_T, pCO_2 + A_T, and SeaFET + A_T calculated DIC data sets were compared to the nine discrete DIC samples taken during two days of the study (Fig. 3.2). The discrete samples covered the full range of DIC on the reef during this deployment.

2.5.2 Gas exchange with the atmosphere

Gas exchange between the ocean and the atmosphere affects the pH, pCO_2, and DIC of the seawater. The air-sea flux (F_{CO2}) calculation is shown in Equation 2.6. The solubility of CO_2 (s) is a function of temperature and salinity (Weiss, 1974). The gas transfer velocity (k) was calculated from a wind speed dependent model (Ho et al., 2006). The difference between the pCO_2 of the seawater (pCO_{2sw}) and the partial pressure of CO_2 in the atmosphere (pCO_{2air}) is calculated from surface ocean seawater and the air in Kaneohe Bay. A positive F_{CO2} represents a net flux of CO_2 from the water to the atmosphere. Gas exchanged is used in net ecosystem production calculations as discussed below.

$$F_{CO2} = k\ s\ (pCO_{2sw} - pCO_{2air}) \hspace{4cm} (2.6)$$

2.5.3 Net ecosystem calcification

For measurements of Net Ecosystem Calcification (NEC) and Net Ecosystem Production (NEP) A_T and DIC were normalized to salinity = 35 (nA_T and nDIC). The average salinity of the open ocean source water (HOT) and at CRIMP-2 was the same (35.2) indicating that terrestrial effects did not alter the A_T of Kaneohe Bay.

A_T is primarily a measure of $[HCO_3^-]$ and $[CO_3^{2-}]$ (Eqn. 1.8). Calcification and dissolution on the reef alter the A_T in the water by removing or adding CO_3^{2-}. NEC is the rate at which the reef community alters the seawater chemistry due to calcification and dissolution (Eqn. 2.7). NEC was calculated using the alkalinity anomaly technique (Smith and Key, 1975). Calcification and dissolution on a coral reef change the alkalinity of the surrounding seawater; for every one mole of $CaCO_3$ formed by calcification, DIC decreases by one mol (Eqn. 1.7) and A_T decreases by two moles (Eqn. 1.8).

$$NEC = \Delta A_T\ h\ \rho\ /\ 2\Delta t \hspace{4cm} (2.7)$$

$$\Delta A_T = A_{T(HOT)} - A_{T(CRIMP)} \hspace{4cm} (2.8)$$

ΔA_T is the difference between open ocean source water $A_{T(HOT)}$ and bay water overlying the reef at CRIMP-2 (Eqn. 2.8). In Equation 2.7 h is the average depth of the water on the reef (2 m), ρ is the density of seawater (kg m^{-3}), and Δt is the residence time of the water on the reef at CRIMP-2. NEC is expressed in mmol $CaCO_3$ m^{-2} h^{-1}. The typical seasonal value of A_T measured at the Hawaiian Ocean Time-series (HOT) station

ALOHA was used to represent open ocean source water. These data was accessed through the HOT Data Organization and Graphical System (HOT-DOGS). The mean A_T from May – August 2013 of 2309 ± 10 μmol kg^{-1} was used for $A_{T(HOT)}$ in the NEC calculations.

The residence time of the water (Δt) was estimated using the width of the reef (2433 m) (Shamberger et al., 2011) and current velocity (m s^{-1}). Wave height was converted to current velocity using a linear relationship given in Lowe et al., (2009a). A distinct tidal signal remained in Δt when Δt was calculated this way, so the calculated values were averaged, resulting in a residence time of 4 hours that was used for the duration of this study. The four hour average was comparable to the June residence time of 4.5 hours reported in Shamberger et al., (2011), and resulted in similar calculated NEC and NEP to those reported in other studies of Kaneohe Bay (Kinsey, 1985, Shamberger et al., 2011). This method of an average Δt still results in a tidal signal in the NEC and NEP records where the reef alters the chemistry of the water as the tide comes in and again when it goes out. It is important to recognize that these are averaged values for Δt that do not account for hourly deviations due to differences wave height, wind and wave direction, wind speed, and tidal amplitude (Lowe et al., 2009a).

2.5.4 Net ecosystem production

Unlike A_T variability, changes in the DIC are affected by photosynthesis, respiration, and gas exchange. Net ecosystem production (NEP) is calculated by removing NEC and gas exchange contributions to the ΔDIC (Eqn. 2.9). ΔDIC is the difference in DIC between the source water (HOT) and the bay (CRIMP-2 site) (Eqn.

2.10). The mean salinity normalized DIC value from June – August 2013 from HOT was 1998 ± 5 µmol kg^{-1}. NEP is expressed in units of mmol C m^{-2} h^{-1}.

$$NEP = (\Delta DIC \ h \ \rho \ / \ \Delta t) - NEC + F_{CO2} \qquad (2.9)$$

$$\Delta DIC = DIC_{(HOT)} - DIC_{(reef)} \qquad (2.10)$$

Ecosystem respiration rates (R) were calculated as the average of the hourly nighttime NEP (when PAR = 0) from the preceding and following nights multiplied by 24 (Falter et al., 2001) (Eqn. 2.11). This approach assumes that rates of daytime and nighttime respiration are equal, an assumption consistent with ecosystem production rates (P) and R calculations on reef flats including Kaneohe Bay (Gattuso et al., 1998; Falter et al., 2011). Gross primary production (GPP) was calculated by integrating daily NEP when PAR > 0 and adding that to hourly rates of community respiration (Eqn. 2.12).

$$R = (\Delta DIC \ h \ \rho \ / \ \Delta t) - \text{Residual nighttime NEC} - F_{CO2} \qquad (2.11)$$

$$GPP = NEP + R \qquad (2.12)$$

2.5.5 Statistical Analysis

Analysis in Matlab of measurements or variables that should have the same value, e.g. two measured pH time series, or measured vs. calculated pCO$_2$, was done using 1:1 lines, lines of best fit, slopes, and residual errors. When comparing possibly unrelated variables, linear regression analysis was performed in Matlab to examine the variance in

e.g. NEC, NEP, and the inorganic carbon speciation. Best-fit (least squares) functions

were determined using 'fitlm' in matlab. Pearson correlation coefficients were used to

identify correlation between paired variables such as light, temperature, Ω_{arag}, and NEP

with p-values to assess the significance of each correlation coefficient.

CHAPTER 3

In situ data and the CO_2 System

3.1 Overview

As stated above, the CRIMP-2 buoy platform had four autonomous sensors measuring three of the CO_2 system parameters during this deployment. Heretofore, only pH and pCO_2 could be measured in situ; this combination does not accurately estimate A_T or DIC in a reef environment. With three measurements, we can more rigorously address the question of sensor performance by comparing the calculated and measured values. More specifically, we took this unique opportunity to (1) examine the robustness of the sensor measurements, (2) compare the resulting CO_2 system calculations from each possible combination of sensors, and (3) assess these comparisons to determine the best data sets to use in further examinations of the biogeochemistry of the reef during this study. In Chapter 4, I evaluate the A_T data in terms of reef calcification and productivity. pH and pCO_2 vary congruently because they are largely controlled by the same processes of production and gas exchange (Cullison Gray et al., 2011). H_2CO_3 regulates H^+ and is regulated by H^+. These processes of NEP and gas exchange affect A_T very little, and A_T variability is mostly due to the balance of precipitation and evaporation, calcification and water mass movement. When using any two parameters to calculate the carbonate equilibria, the combination of parameters DIC or A_T with either pH or pCO_2 minimize errors (Clayton et al., 1995; Lee and Millero, 1995; McElligott et al., 1998; Byrne et al., 1999; Lee et al., 2000; Cullison Gray et al., 2011), so the SAMI-alk data was used in all three of the possible combinations with pH and pCO_2 (Sami-alk with SAMI-pH, SeaFET, and MAPCO2). Carbonate equilibrium calculations using pH and pCO_2 were also

25

evaluated in order to further explore the consensus that they are not an appropriate

combination of measurements in a coral reef environment.

3.2 Results

3.2.1 Measured parameters

Despite our best attempts at timing the sensors so that they sampled the same

seawater, all four sensors sampled at slightly different times. For this comparison the

SeaFET and MAPCO2 data were interpolated to the time of the SAMI-alk samples. This

was not necessary for the SAMI-pH because it sampled at such a high rate that it did

sample at the same time as the SAMI-alk. The measured (not interpolated) pCO$_2$ and

both measured (not interpolated) pH records are presented in Fig. 3.1.
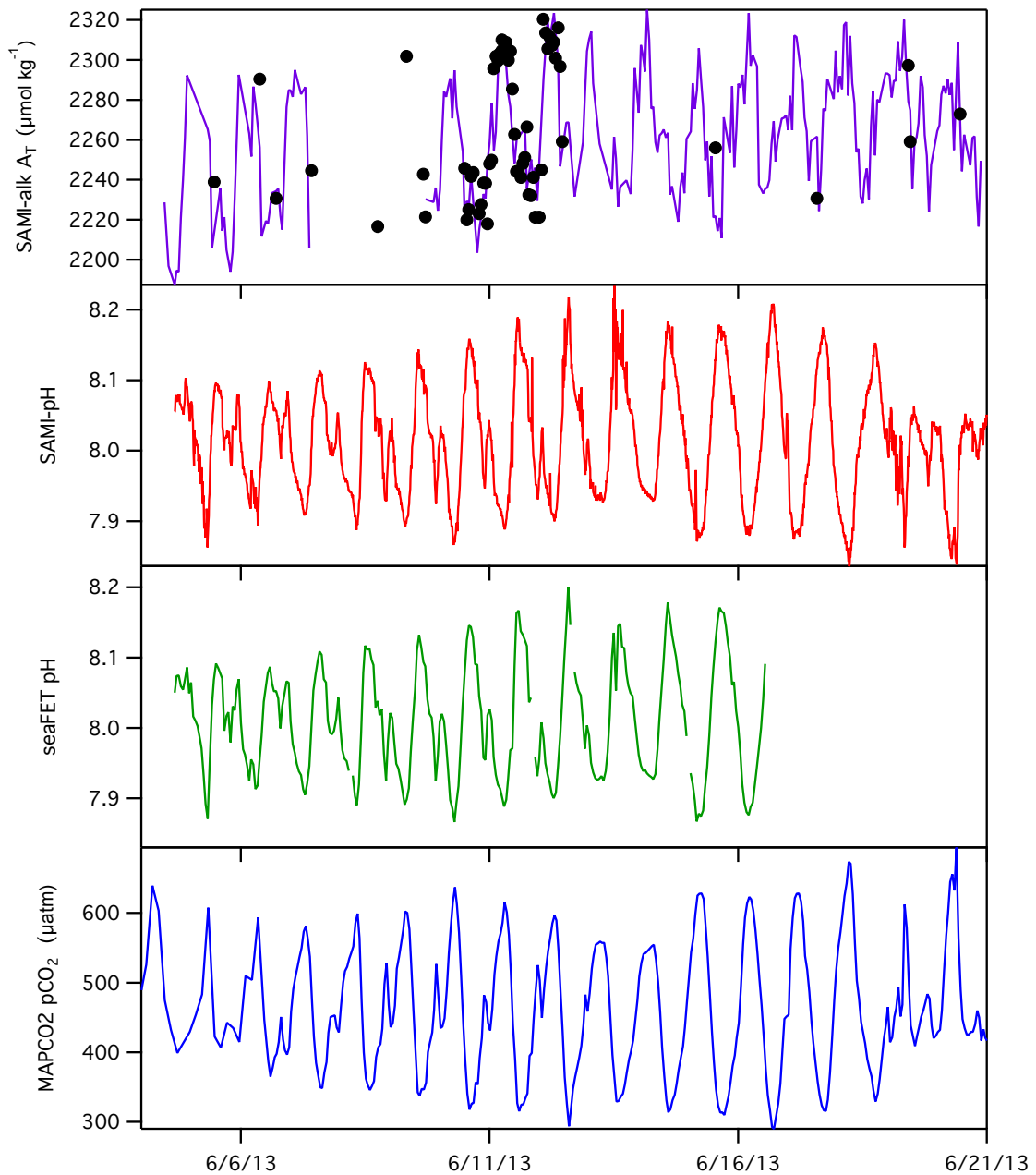
Figure 3:1 A_T measured by the SAMI-alk (purple) with discrete samples (black dots), pH measured by the SAMI-pH (red), SeaFET with the applied offset (see text) (green), and pCO_2 measured by the MAPCO2 system (blue) during the study June 4 – 21. The SAMI-pH measuring every 10 minutes captured short-term variability missed by the instruments measuring hourly as seen in the MAPCO2 record, e.g. around 6/14/ see the greater variability in pH compared to pCO_2.

3.2.2 Calculated parameters: A_T, DIC, pH and pCO$_2$

The three calculated DIC data sets are plotted in Figure 3.2. In addition to the two measured pH records, pH was calculated using the $A_T + p$CO$_2$ combination. Similarly, pCO$_2$ was measured (MAPCO2) and calculated two ways: A_T + SAMI-pH and A_T + SeaFET. The calculated and measured DIC, pH and pCO$_2$ are plotted in Figure 3.2.
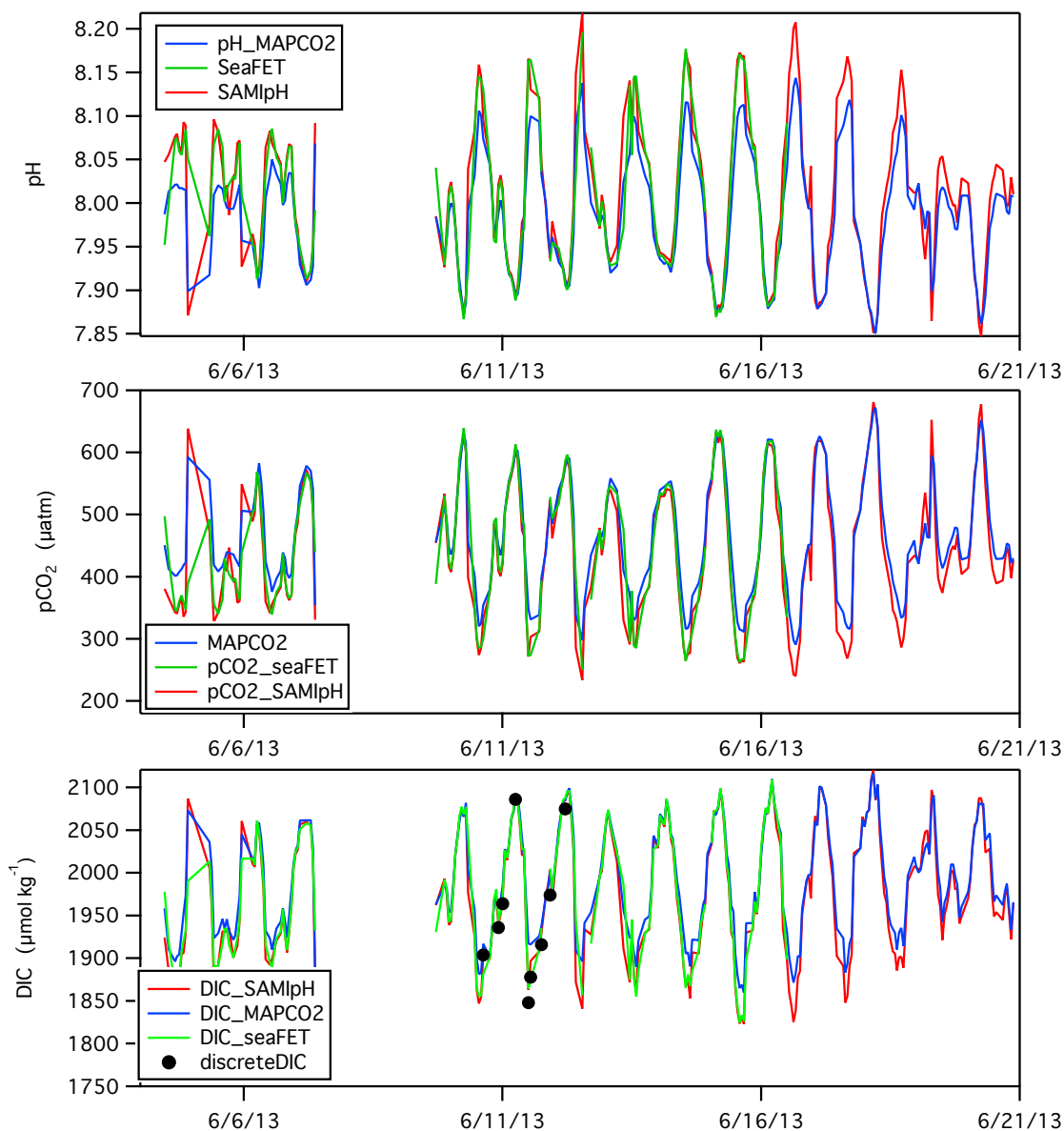
Figure 3:2 pH measured from the SAMI-pH and SeaFET, and calculated from the pCO$_2$ + A$_T$ (top), pCO$_2$ measured from the MAPCO2 system and calculated from SAMI-pH + A$_T$, and SeaFET + A$_T$ (middle), and DIC calculated from the SAMI-pH + A$_T$, SeaFET + A$_T$, and pCO$_2$ + A$_T$ (bottom) with discrete DIC points in black. The two days of missing data are from a SAMI-alk software error.

Only data from June 10 on were used for all measured parameter comparisons (pH vs.

pH, pCO$_2$ vs. pCO$_2$, etc.). Before June 10 the SeaFET, and MAPCO2 sampled every 3

hours instead of hourly. With the large diel swings observed in this study, interpolation over 3 hours was not representative of the measured variability.

A_T was also calculated using the SAMI-pH + pCO$_2$ combination and compared to the measured A_T from the SAMI-alk and the discrete A_T samples (Fig. 3.3). As stated above, the pH + pCO$_2$ pair results in the largest errors when calculating carbonate equilibria as shown in Figure 3.3. Large and unrealistic values of A_T are created from a lack of correlation between pH and pCO$_2$, that is, if pCO$_2$ changes but pH does not, e.g. due to an error in pCO$_2$, then this has to result in a large change in A_T to account for this uncorrelated change. These can be created by, for example, measurement timing differences during rapidly changing signals. As shown in Figure 3.3, some very large errors are present, rendering the data unusable, when the signals are changing rapidly. Statistics from these differences are presented below.
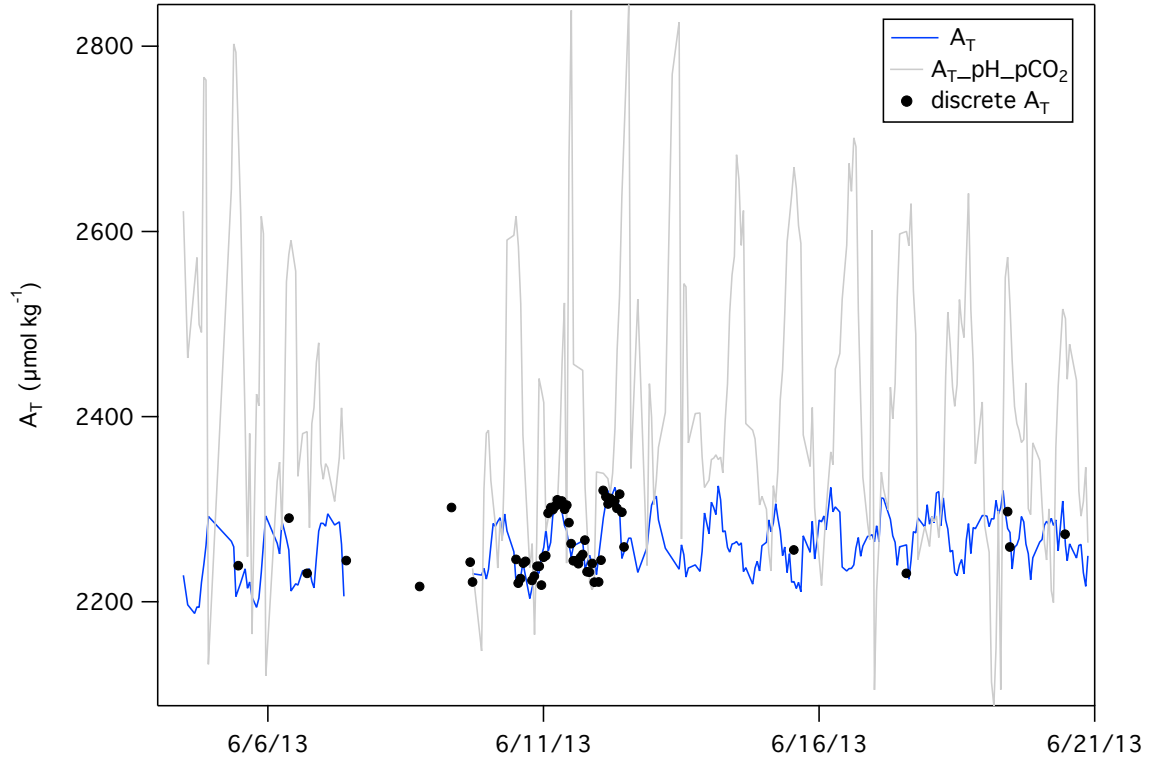
Figure 3:3 A_T measured from the SAMI-alk (blue) and calculated from the SAMI-pH + pCO_2 (grey), with discrete A_T points (black).

3.2.3 pH comparison

When the three pH time series were initially plotted the SeaFET pH was consistently lower than both the SAMI-pH and the pH calculated from the $A_T + pCO_2$ combination. A constant offset of + 0.08 pH units was applied to the SeaFET data based on the two other time series in lieu of a calibration because the SAMI-pH and MAPCO2 values were consistent with each other for all but low values. A single point calibration is recommended for the SeaFET (Martz et al., 2010; Bresnahan et al., 2014).

The three combinations of pH are compared in Figure 3.4 below and the results are summarized in Table 3.1. The data from the SAMI-pH and offset-corrected SeaFET fall closest to 1:1 with a slope of 0.98, ($r^2 = 0.94$), but as the SeaFET was calibrated to the

SAMI-pH we expect the slope to be very close to 1 unless there is drift or biofouling. The SAMI-pH and the pH calculated from the $A_T + pCO_2$ combination has the least amount of scatter ($r^2 = 0.96$) and a slope of 0.79, which significantly deviates from the 1:1 line specifically at high pH. The relationship between the SeaFET and the pH calculated from the $A_T + pCO_2$ is farthest from 1:1 with a slope of 0.77, ($r^2 = 0.94$). The two combinations with the SeaFET have slightly lower r^2 values (Table 3.1). The SeaFET also has the most scatter in the data; it has a lower reported accuracy and experienced biofouling.
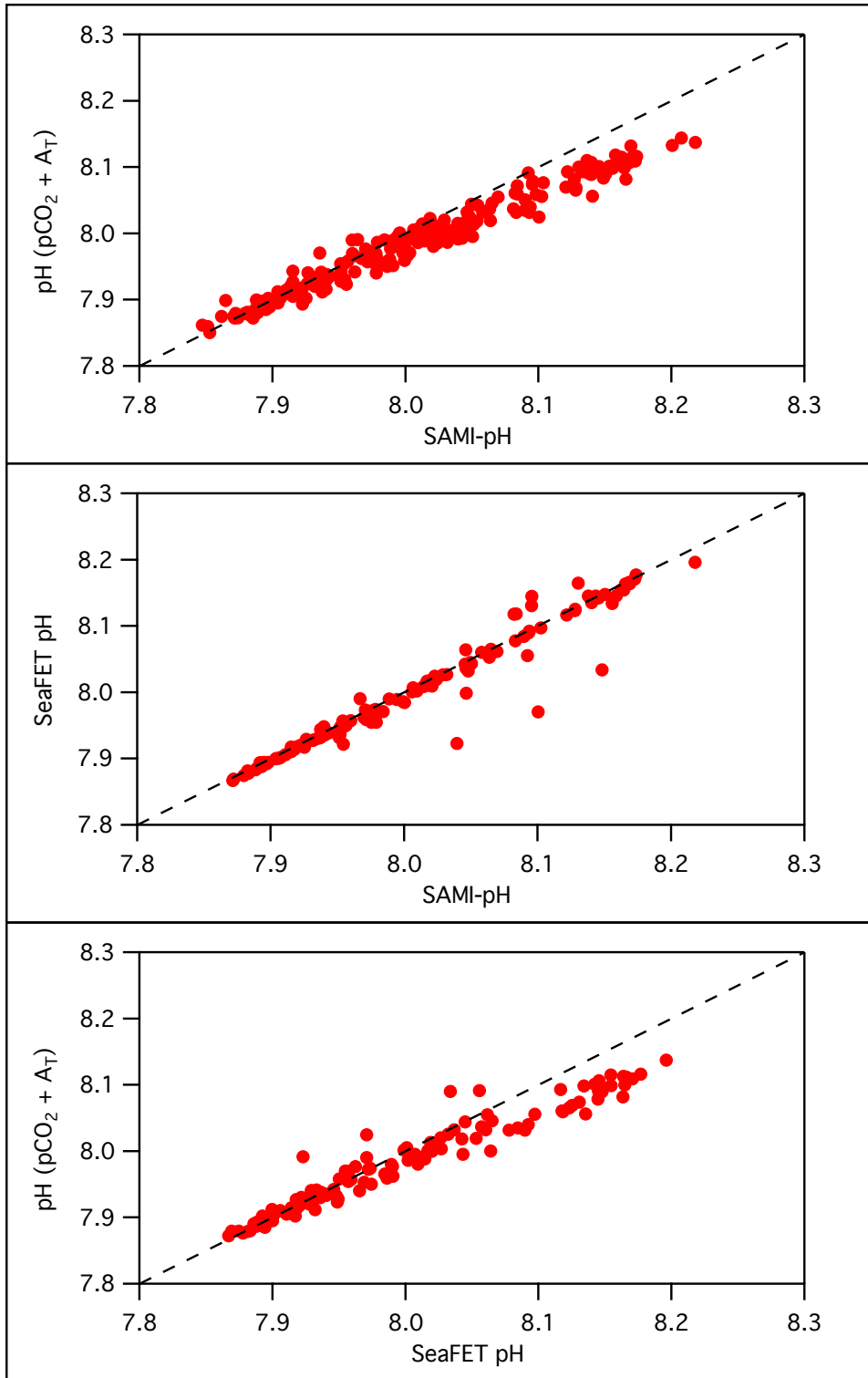
Figure 3:4 Comparisons of SAMI-pH vs. pH calculated from pCO$_2$ + A$_T$ (top), SAMI-pH vs. SeaFET (middle), and SeaFET vs. pH from pCO$_2$ + A$_T$ (bottom). Dashed line represents 1:1.

Table 3.1 Summary of slope and r^2 values of three pH comparisons.

	slope	r^2	n
SAMI-pH vs. pH from $pCO_2 + A_T$	0.79	0.96	215
SAMI-pH vs. SeaFET	0.98	0.94	123
SeaFET vs. pH from $pCO_2 + A_T$	0.77	0.94	123

3.2.4 pCO_2

The best agreement between pCO_2 data sets comes from the calculated pCO_2 from the SAMI-alk and either pH sensor (Fig. 3.5, Table 3.2). This relationship has a slope of 0.99 and an $r^2 = 0.95$. The slope of the relationship between the measured MAPCO2 and pCO_2 calculated from the SAMI-pH + A_T is 0.85 and $r^2 = 0.97$. The slope of the MAPCO2 pCO_2 and the pCO_2 from the SeaFET + A_T is 0.83 and $r^2 = 0.95$. These results are summarized in Table 3.2. Note that the linear relationship between measured pCO_2 (MAPCO2) and calculated (SAMI-pH or SeaFET + A_T) pCO_2 lies closest to the 1:1 line at high values of pCO_2 and deviates at low values of pCO_2.

Table 3.2 Summary of slope and r^2 values of three pCO_2 comparisons.

	slope	r^2	n
pCO_2 from SAMI-pH + A_T vs. MAPCO2	0.85	0.97	215
pCO_2 from SAMI-pH + A_T vs. pCO_2 from SeaFET + A_T	0.99	0.95	123
pCO_2 from SeaFET + A_T vs. MAPCO2	0.83	0.95	123
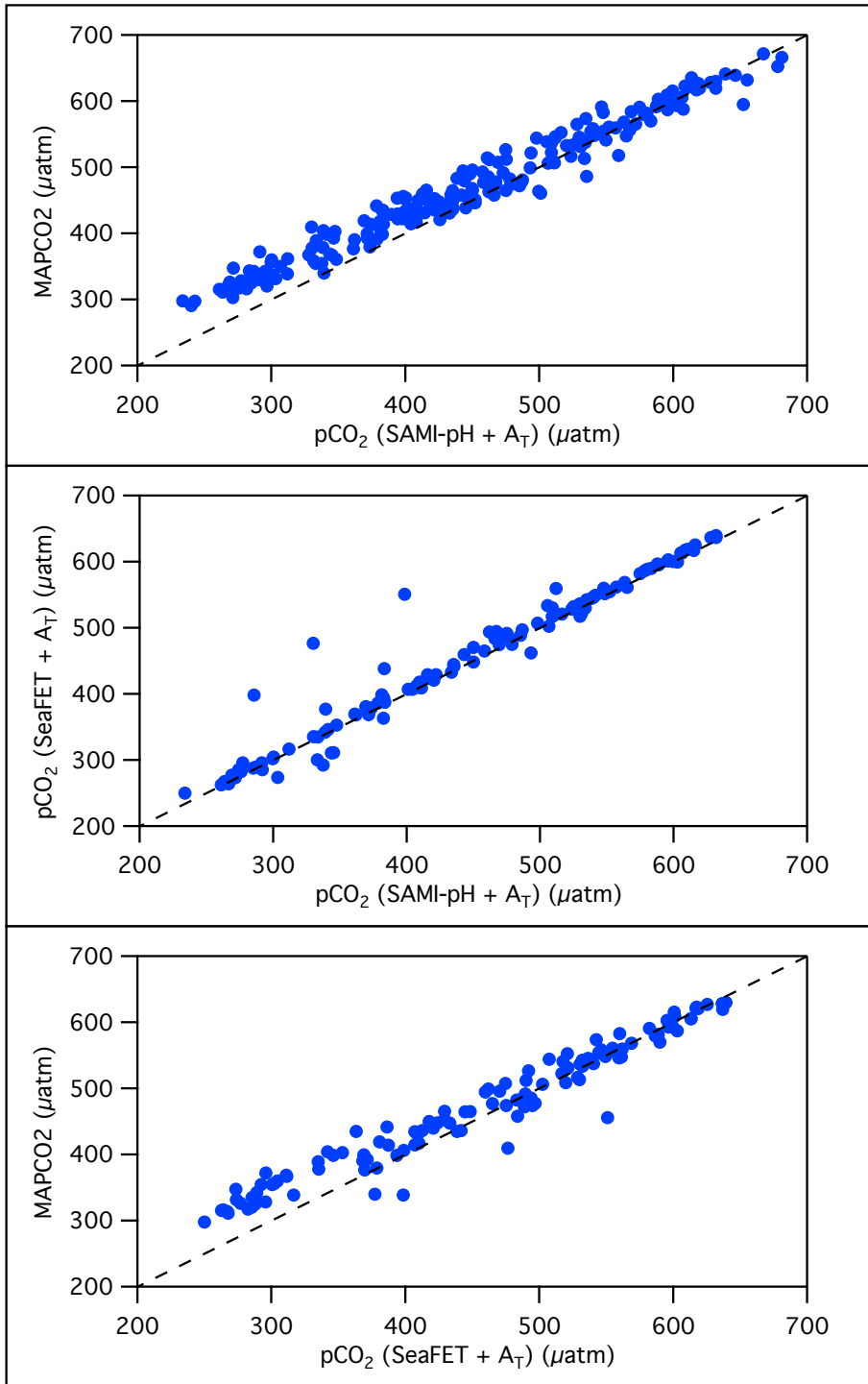
Figure 3:5 Comparisons of pCO$_2$ (µatm) from SAMI-pH +A$_T$ vs. MAPCO2 (top), pCO$_2$ from SAMI-pH + A$_T$ vs. pCO$_2$ from SeaFET + A$_T$ (middle), and pCO$_2$ from SeaFET + A$_T$ vs. MAPCO2 (bottom). Dashed line represents 1:1.

3.2.5 DIC

I compared the calculated DIC values with each other (Fig. 3.6) in addition to comparing the three calculated DIC data sets with measured DIC from bottle samples (Fig. 3.7, 3.13). Figure 3.6 shows each comparison plot and Table 3.3 summarizes the slope and r^2 values. The DIC from the SAMI-pH + A_T vs. the DIC from the SeaFET + A_T have a slope of 0.98 and an $r^2 = 0.97$. The DIC from the SAMI-pH A_T vs. the DIC from the pCO_2 + A_T have a slope 0.85 and an $r^2 = 0.98$. The DIC from the SeaFET + A_T vs. the DIC from the pCO_2 + A_T have a slope of 0.85 and an $r^2 = 0.97$. We can assume that any error generated by the SAMI-alk is the same in all three DIC calculations so the differences in DIC are caused by something else.

Table 3.3 Summary of slope and r^2 values of three DIC comparisons.

	slope	r^2	n
DIC from SAMI-pH + A_T vs. DIC from pCO_2 + A_T	0.85	0.98	215
DIC from SAMI-pH + A_T vs. DIC from SeaFET + A_T	0.98	0.97	123
DIC from SeaFET + A_T vs. DIC from pCO_2 + A_T	0.85	0.97	123
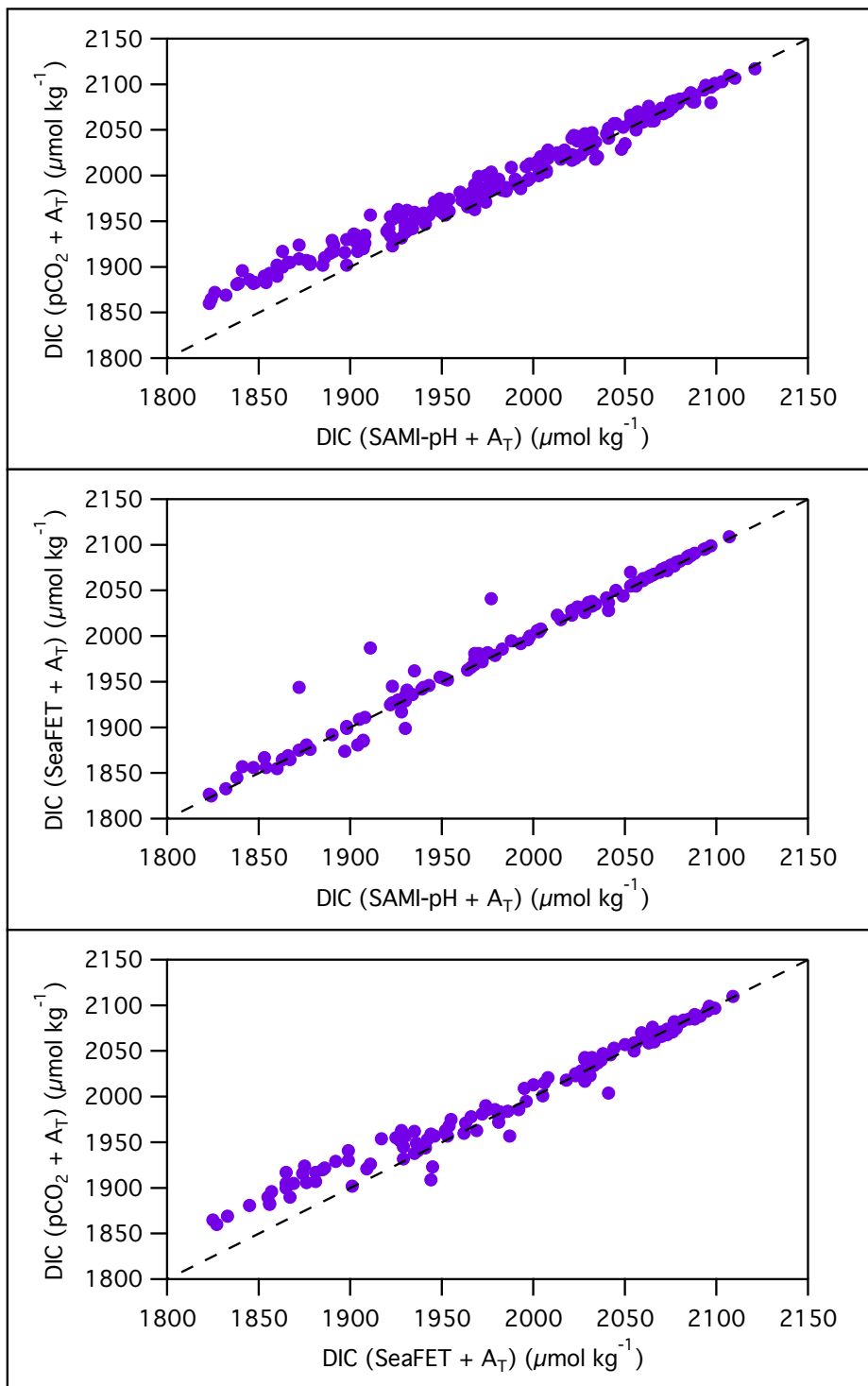
Figure 3:6 Comparisons of DIC (μmol kg^{-1}) calculated from SAMI-pH + A$_T$ vs. DIC from pCO$_2$ + A$_T$ (top), DIC from SAMI-pH + A$_T$ vs. DIC from SeaFET + A$_T$ (middle), and DIC from SeaFET + A$_T$ vs. DIC from pCO$_2$ + A$_T$ (bottom). Dashed line represents 1:1.

3.2.4 DIC by calculation and measurements of discrete samples

We took 9 discrete seawater samples and analyzed them for DIC over the course of June 10 – 12. These 9 samples covered the full diel cycle, including points at both high and low DIC (Fig. 3.7). The three calculated DIC data sets are compared with the measured DIC in Figure 3.7 (top and bottom). The mean difference (measured-calculated ± SD) between the sample DIC and the calculated DICs are shown in Table 3.4. (Fig. 3.7, Table 3.4).
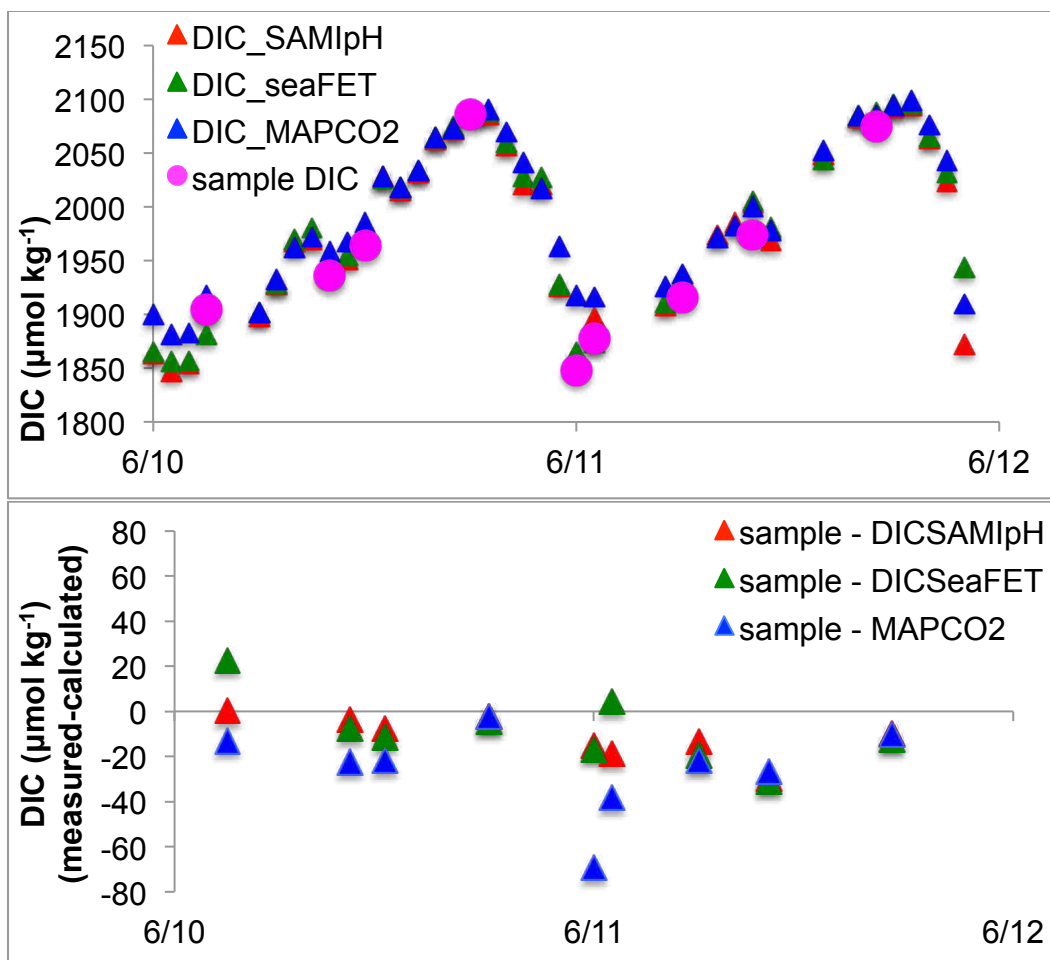
Figure 3:7 48 hours of DIC (μmol kg^{-1}) calculated from A_T and SAMI-pH, SeaFET, and MAPCO2 with 9 discrete measured DIC samples (top), and DIC calculated from A_T and SAMI-pH, SeaFET, and MAPCO2 subtracted from discrete DIC samples (measured-calculated) (n = 9) (bottom).

Table 3.4 Difference in sample DIC and DIC calculated from the three parameters of pH and pCO$_2$.

	mean difference (**measured-calculated**) in DIC (μmol kg^{-1})	standard deviation
DIC from SAMI-pH + A_T	- 11	± 9 (n = 9)
DIC from SeaFET + A_T	- 9	± 15 (n = 9)
DIC from pCO$_2$ + A_T	- 25	± 19 (n = 9)

3.3 Discussion

3.3.1 pH – pCO$_2$ pair calculations
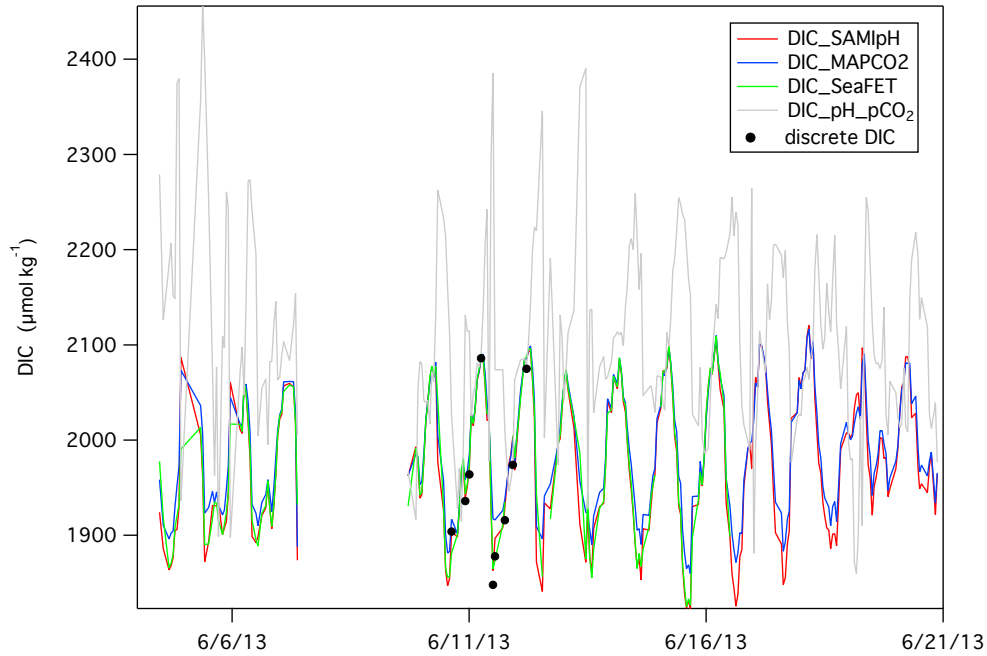
Figure 3:8 DIC calculated four ways plotted with discrete DIC samples (black dots).

As demonstrated above (Figs. 3.2, 3.8), the carbonate system calculations from the pH + pCO$_2$ pair result in the largest calculation errors. With this approach, calculated DIC and A_T differed from measured (by discrete sample) DIC and A_T by up to 300 and 500 µmol kg^{-1}, respectively. This calculation pairing even failed at times to predict the proper diel phase of A_T and DIC; calculated DIC and A_T increased while measured DIC and A_T decreased (Figs. 3.2, 3.8). pH and pCO$_2$ are temperature, pressure, and salinity dependent so calculations with this pair will predict erroneous results when pH and pCO$_2$ do not track with temperature, salinity or pressure (Millero, 2007).
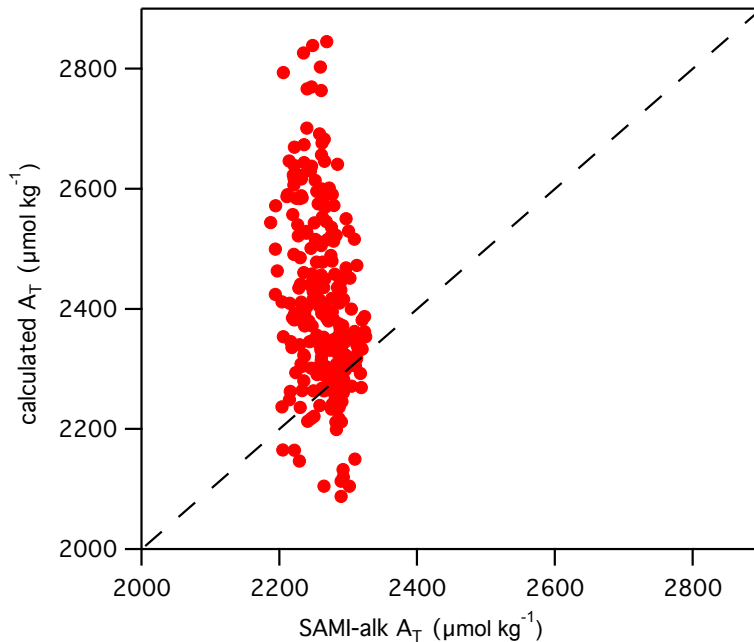
Figure 3:9 A_T measured by the SAMI-alk vs. A_T calculated from the SAMI-pH + MAPCO2 pair (pH + pCO$_2$). Dashed line represents 1:1.

In this study, the pH + pCO$_2$ calculations are particularly sensitive because processes such as calcification and production drastically alter the seawater chemistry on a short, hourly timescale. Calculation errors will result any time pH and pCO$_2$ are not correlated, or when they are changing rapidly (Cullison Gray et al., 2011). This happens frequently and thus the A_T calculated from the pH and pCO$_2$ plotted vs. measured A_T (from the SAMI-alk) do not fall on a 1:1 line (Fig. 3.9). The pairing can still be useful where the A_T of the ocean is conservative with salinity (Cullison Gray et al., 2011), but in a reef ecosystem where A_T changes rapidly due to calcification pH and pCO$_2$ cannot be used in combination to calculate A_T or DIC.

There is one potential useful aspect of the pH + pCO$_2$ paring in CO$_2$ system calculations. Most of the DIC in seawater is present as HCO_3^-, in fact 90% of inorganic carbon is in the HCO_3^- form at pH 8.0. Because very little inorganic carbon in seawater is

present as CO_3^{2-}, calculations such as aragonite saturation state (Eqn. 1.9) (Ω_{arag}) are less sensitive to errors using the pH + pCO$_2$ combination (Cullison Gray et al., 2011). Figure 3.10 shows Ω_{arag} calculated two ways. The Ω_{arag} using the pH – A$_T$ combination agrees closely with the Ω_{arag} using the pH + pCO$_2$ pair at all but high values of Ω_{arag}. These high values correspond to low values of pCO$_2$ where there is potential error in the MAPCO2 system's measurements, as discussed below. The mean difference ± standard deviation of the Ω_{arag} from the pH – A$_T$ pair minus the pH – pCO$_2$ pair is -0.25 ± 0.27. If the high values of Ω_{arag} (low values of pCO$_2$) are removed from the SAMI-pH + pCO$_2$ pair, the mean difference improves (-0.12 ± 0.15). Measured pCO$_2$ errors are discussed in detail later in this chapter. Because the Ω_{arag} from the pH + pCO$_2$ combination matches the Ω_{arag} from the SAMI-pH + A$_T$ combination, the pH + pCO$_2$ pair may provide reasonable estimations of Ω_{arag}, but is not conclusive because of the issues with the MAPCO2 measurements discussed below.
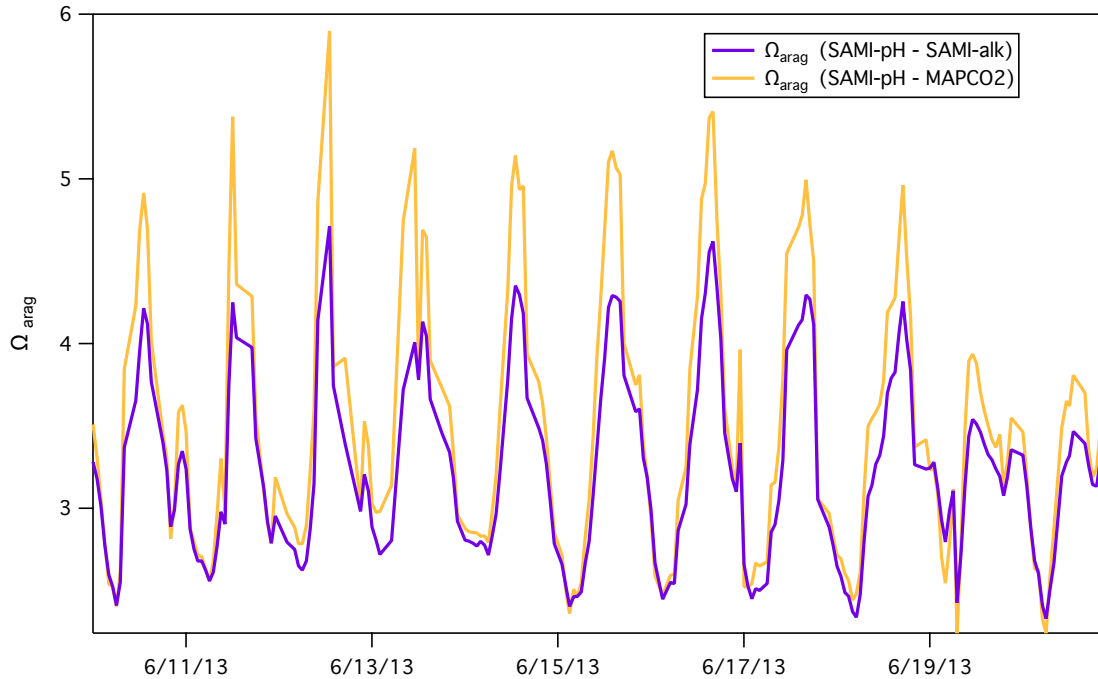
Figure 3:10 Ω_{arag} calculated using the SAMI-pH – SAMI-alk pairing (pH – A_T, purple), and the SAMI-pH – MAPCO2 pairing (pH – pCO$_2$, yellow).

3.3.2 A_T + pH and A_T + pCO$_2$ pair calculations

The quality of the A_T data has an influence on the other three calculation pairs (A_T with SAMI-pH, SeaFET, and MAPCO2). An evaluation of the accuracy of the SAMI-alk is included in Spaulding et al., (2014). If there were a systematic error in A_T it would show up in all three calculated data sets and thus be hard to detect. But we would also see it when comparing the calculated DIC using the SAMI-alk data with the sampled DIC (Fig. 3.7). Errors in A_T propagate as errors of the same magnitude in DIC (a 10 µmol kg^{-1} error in A_T will result in a ~10 µmol kg^{-1} error in DIC at the same pH or pCO$_2$). Whereas, a pH error of 0.02 or a pCO$_2$ error of 20 µatm could result in a DIC error of 150 µmol kg^{-1} (Cullison Gray et al., 2011). A systematic offset (seen over the whole range of measured

DIC) between the discrete sample DIC and any of the 3 calculated DIC data sets is not present in these data (Fig. 3.7); they agree better at high DIC for DIC calculated from the $pCO_2 + A_T$ pair, but not for the other two pairings (Fig. 3.13).

The three plotted pCO_2 time series reveal an interesting feature – while the pCO_2 calculated from the SAMI-alk and both pH sensors overlaps over the full diel cycle, the MAPCO2 measured pCO_2 does not drop as low each day (Fig. 3.2 middle); the calculated pCO_2 from the two pH + A_T combinations is at times 60 μatm lower than the measured pCO_2 (Fig. 3.2 middle, blue line). This is also apparent in the calculated pH and DIC from the $pCO_2 + A_T$ calculations: the calculated pH is not as high as the measured pH (Fig. 3.2 top) and the calculated DIC does not drop as low as the DIC calculated from the two other sensor calculations (Fig. 3.2 bottom). The discrepancy is only observed when the pCO_2 changes from decreasing to increasing, not simply when it is below a certain value (Fig. 3.11). The discrepancy also occurs when the pCO_2 is both below and above atmospheric pCO_2 (dotted line on Fig. 3.11). The SeaFET was calibrated to the SAMI-pH so it is expected that they agree very well, however that calibration would not affect the range of variability measured by the SeaFET. The range of variability measured by the SeaFET and SAMI-pH is the same, but the range of variability from the MAPCO2 is not.
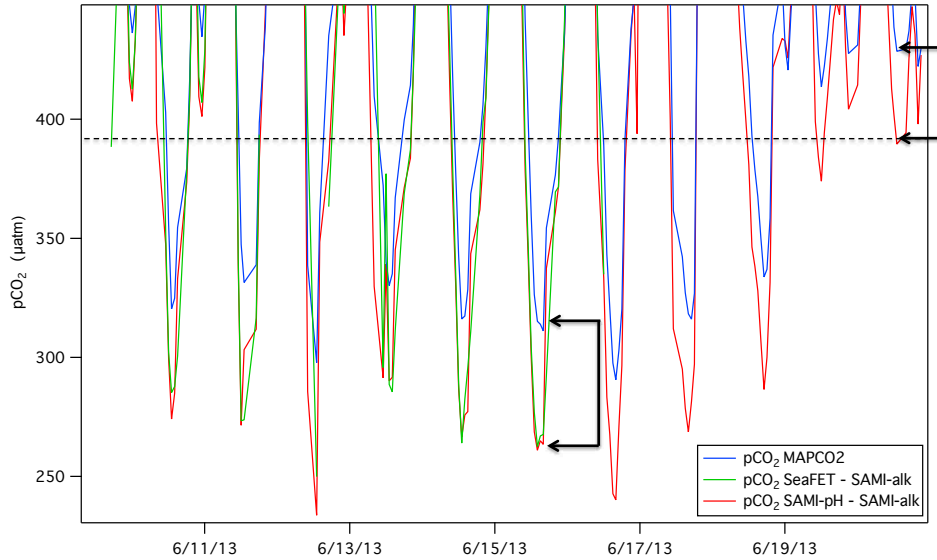
Figure 3:11 Expanded view of pCO_2 measured or calculated. Dashed line shows atmospheric pCO_2. Arrows indicate differences in measured pCO_2 (MAPCO2) and calculated ($pH - A_T$) pCO_2 both below and above atmospheric pCO_2.

The mean difference between each set of measurements (SAMI-pH, MAPCO2, SeaFET) for each CO_2 system parameter (pH, pCO_2, DIC) is presented in Table 3.5, where the largest differences come from parings involving the MAPCO2 system. Remember the SeaFET time series was truncated because of biofouling. These trends are more clearly shown with difference plots (Fig. 3.12) i.e. the difference between the pH measured by the SAMI-pH and the SeaFET, and the difference between the pH from the SAMI-pH and the pH from the $pCO_2 - A_T$ pair (Fig. 3.12 top). The difference between any two pH pairings would be zero if the measurements were in perfect agreement (Table 3.5, Fig. 3.12), but this is not the case. The difference between the pH from the SAMI-pH and the SeaFET is evenly distributed above and below zero with outliers coming from scatter in the SeaFET, as it is seen only in combinations with the SeaFET. However, the difference between the pH from the SAMI-pH and the $pCO_2 + A_T$ pair is almost always

positive: $((\text{SAMI-pH}) - (p\text{CO}_2 + \text{A}_\text{T} \text{ pair})) > 0$. This difference is greatest at high pH,

where the SAMI-pH measures higher than the pH calculated from MAPCO2. The offset

at high pH corresponds to low $p\text{CO}_2$; the highest SAMI-pH measurements correspond to

the lowest $p\text{CO}_2$ measurements – where the MAPCO2 is not measuring as low as the

other sensors (Fig. 3.11, Fig. 3.12 middle).

Table 3.5 Mean differences in pH, $p\text{CO}_2$ and DIC as measured directly or calculated from pH – A_T, or $p\text{CO}_2$ – A_T pairs from each of the three sensors reported as mean ± standard deviation.

	pH	$p\text{CO}_2$	DIC	n
SAMI-pH – MAPCO2	0.020 ± 0.023	-21 ± 25	-12 ± 14	215
SAMI-pH –SeaFET	0.006 ± 0.022	-8 ± 25	-3 ± 13	123
SeaFET –MAPCO2	0.016 ± 0.027	-16 ± 29	-10 ± 17	123
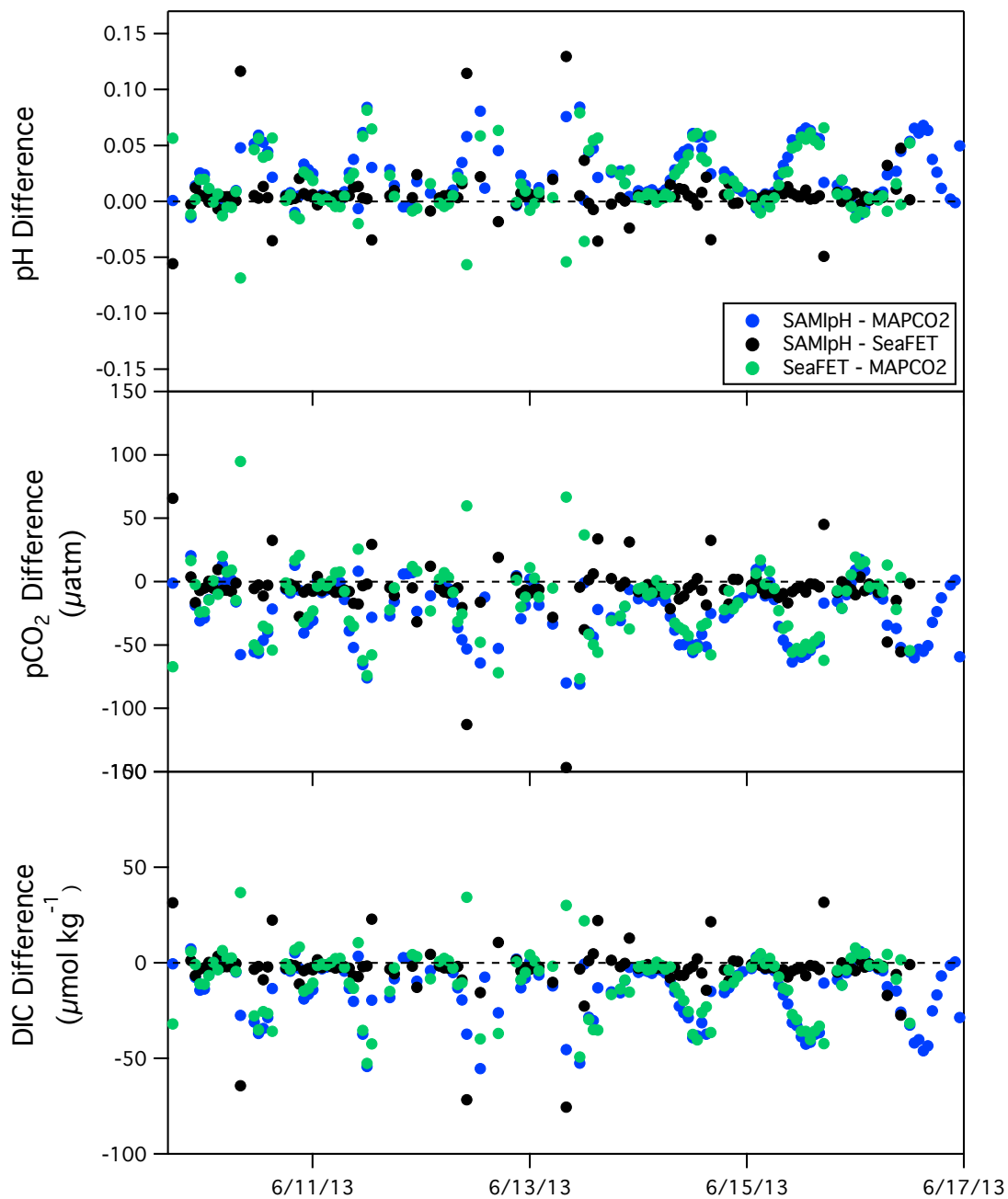
Figure 3:12 Top: difference in pH from the SAMI-pH – (pCO$_2$ + A$_T$) pair (blue), SAMI-pH – SeaFET (black), and SeaFET – (pCO$_2$ + A$_T$) pair (green). Middle: difference in pCO$_2$ from the (SAMI-pH + A$_T$) pair – MAPCO2 (blue), (SAMI-pH + A$_T$) pair – (SeaFET + A$_T$) pair (black), and (SeaFET + A$_T$) pair – MAPCO2 (green). Bottom: difference in DIC from the (SAMI-pH + A$_T$) pair – (pCO$_2$ + A$_T$) pair (blue), (SAMI-pH + A$_T$) pair – (SeaFET + A$_T$) pair (black), and (SeaFET + A$_T$) pair – (pCO$_2$ + A$_T$) pair (green).

In Figure 3.13, the calculated DIC values are again compared with the sample DIC. For the pCO_2 + A_T pair, the calculated DIC falls off the 1:1 line when DIC is low because the DIC calculated from the pCO_2 + A_T pairing is too high at low DIC (Fig. 3.2 bottom). This corresponds to the low values of pCO_2 where the measured pCO_2 from the MAPCO2 system is higher than the pCO_2 calculated from both pH – A_T pairs (Fig. 3.2 middle). We see the same deviation from the 1:1 line in Figures 3.7 and 3.8 comparing the calculated DIC and measured and calculated pCO_2 data sets with each other. The data matches the 1:1 line at high DIC and pCO_2 better than at low DIC and pCO_2 as said previously. When the two low values of discrete sample DIC are removed from Figure 3.13 the slope and r^2 of the DIC comparisons between sample DIC and DIC calculated from the pCO_2 + A_T improve from 0.82 to 0.92 and r^2 from 0.97 to 0.99 (n = 9 and n = 7, respectively). The mean difference +/- standard deviation between the measured DIC and the DIC calculated from the pCO_2 + A_T drops from -25 ± 19 (Table 3.4) to -17 ± 8 when the two low values of discrete DIC are removed. The correlations of the DIC samples and the DIC calculated from the SAMI-pH and SeaFET were made worse by removing data. This analysis suggests that the MAPCO2 is recording systematically high pCO_2 values when the pCO_2 is changing from decreasing to increasing pCO_2. Some possible sources of error are presented in the following paragraph.
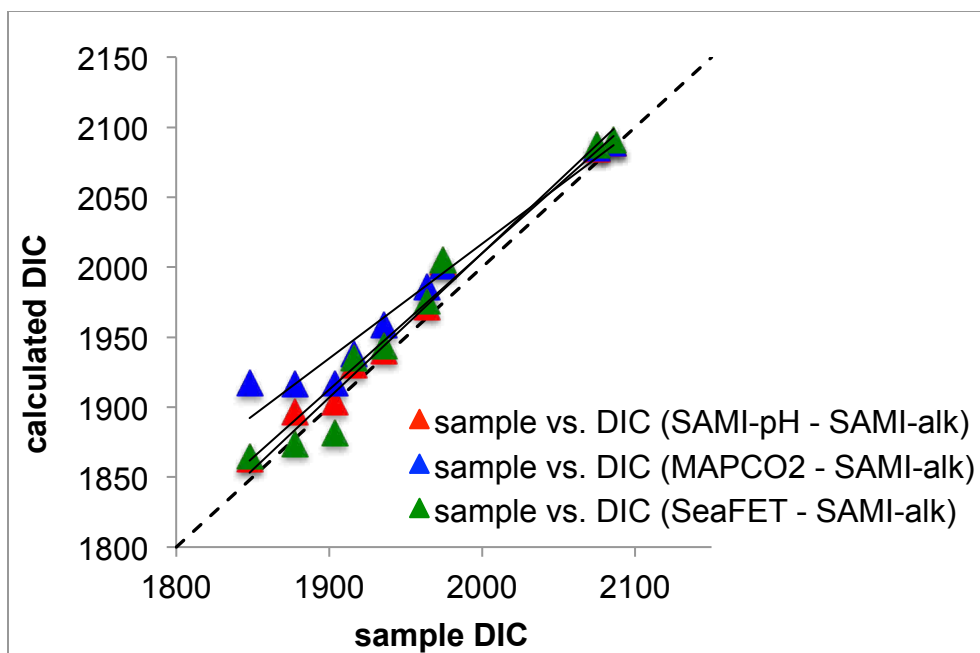
Figure 3:13 Sample DIC (μmol kg^{-1}) vs. DIC from (SAMI-pH +A_T) (red), slope = 0.97, r^2 = 0.98. Sample DIC vs. DIC from (pCO$_2$ + A_T) (blue), slope = 0.82, r^2 = 0.97. Sample DIC vs. DIC from (SeaFET + A_T) (green), slope = 1.03, r^2 = 0.97. Dashed line represents 1:1.

In the MAPCO2 system a closed loop of air circulates through an equilibrator for 10 minutes for each CO_2 measurement (Sutton et al., 2015). Each seawater CO_2 measurement is a result of integrated seawater CO_2 levels during that 10-minute equilibration time. Clearly, the pCO$_2$ of the seawater changes rapidly in Kaneohe Bay (Fig. 3.1 bottom), but if the observed low pCO$_2$ offset were a simple issue with rate of equilibration we would expect an offset whenever pCO$_2$ was changing rapidly, e.g. at higher pCO$_2$ levels the pCO$_2$ would be expected to be systematically lower.

The infrared analyzer (LICOR-820) in the MAPCO2 system is calibrated with a zero gas and a 688 ppm calibrated standard reference gas from NOAA Earth Systems Research Laboratory (ESRL) before each seawater measurement. The zero gas applies an offset to the pCO$_2$ measurements by setting a zero value. A calibration curve is then

applied using the standard gas as a point along the curve from zero. The shape of that curve could fit well at high pCO_2 values – values around and above the standard gas – but not fit well at low values based on similar calibrations our group has run. However, errors of this magnitude are not expected from this type of calibration. If this is the case, the high and mid range values would be very accurate and the low values would be off as we see during this study, but all of the lower pCO_2 values would be off below a certain pCO_2 threshold, which is not the case here. The system is also verified with six gas standards ranging from 0 – 800 ppm both before and after the deployment (Sutton et al., 2015) and no correction was necessary for this deployment.

The seawater pCO_2 value is highly variable relative to atmospheric pCO_2 in Kaneohe Bay (Drupp et al., 2013). Low pCO_2 values are observed when biological activity on the reef consumes CO_2 and produces oxygen (Drupp et al., 2011; Shamberger et al., 2011). When oxygen is oversaturated in the water due to productivity, a positive pressure could form in the equilibrator and then vent by bubble bursting. This would result in a measured pCO_2 that is lower than pCO_2 at equilibrium (Schneider et al., 2007). That loss of gas would require makeup gas to accurately measure pCO_2. If this is the case we could see full equilibration during the measurements at high pCO_2, but not when the pCO_2 is low due to a loss of gas in the equilibrator. Unfortunately, this cannot fully explain the observed differences because we see the pCO_2 discrepancy even at values where we can calculate negative NEP during the day (June 19-20, respiration calculations discussed further in chapter 4).

3.4 Conclusions

These results show that the in situ A_T from the SAMI-alk provides an excellent inorganic carbon parameter from which other parameters can be accurately and precisely calculated. As previously known, we can conclude that the pH + pCO$_2$ pairing is inadequate for CO$_2$ system calculations in this highly variable coral reef environment, although the Ω_{arag} from the pH + pCO$_2$ pairing could still be useful. The DIC from the SAMI-pH + A_T combination has a much higher accuracy than the pCO$_2$ + A_T combination with the same number of samples and a similar, though slightly lower accuracy to the SeaFET + A_T combination with more samples (Table 3.4). The comparison between the sample DIC and the three calculated DIC data sets shows that the DIC calculated from the SAMI-pH + A_T combination has the highest precision (Table 3.4). The best pH comparisons came from those including the SAMI-pH (SAMI-pH vs. SeaFET and SAMI-pH vs. pH from pCO$_2$ + A_T). The SeaFET did not sample during the second half of the deployment due to biofouling, and an offset had to be applied to the data. The pH calculated from the pCO$_2$ + A_T combination missed the peak pH each day. The pCO$_2$ measured from the MAPCO2 system did not drop as low each day as the pCO$_2$ calculated from the A_T and either of the pH sensors. For these reasons, CO$_2$ system calculations from the A_T + SAMI-pH combination were used for further analysis of the reef biogeochemistry in Chapter 4.

Lastly, these data highlight the challenges in quality control (QC) of in situ data. The in situ A_T, combined with pH two ways, and pCO$_2$ allowed us to rigorously compare the measured data and to verify the data quality. The MAPCO2 system was carefully

calibrated both before and after the deployment and the resulting data was submitted to rigorous post deployment QC but were unable to characterize or correct for the observed errors. The discrepancies observed in the measured and calculated pCO_2 would not have been apparent if either pH or discrete DIC had not also been measured and then used to examine the CO_2 system calculations. It is important to note that while the infrared analyzer accuracy is validated using CO_2 standards, there is no practical way to account for errors in the equilibration process (Kortzinger et al., 2000). MAPCO2 systems are widely used, globally, 36 moored stations with MAPCO2 systems are in operation today (Sutton et al., 2018) and so further evaluation of their performance is critical. The autonomous measurement comparisons presented in this chapter highlight the importance of field validation of instrument accuracy. Finally, the autonomous A_T measurements made by the SAMI-alk were crucial because the pH + pCO_2 pairing did not accurately estimate DIC or A_T in this environment.

CHAPTER 4

Kaneohe Bay: A_T variability on a coral reef

4.1 Overview

Coral reef ecosystems rely on marine organisms that use $CaCO_3$ to build their

skeletons. When CO_2 reacts with seawater it decreases the availability of $[CO_3^{2-}]$; as

ocean pH declines so do the saturation states of calcite (Ω_{Ca}) and aragonite (Ω_{arag}), the

two mineral forms of $CaCO_3$ (Eqn. 1.9). Reef ecosystems may be especially vulnerable to

the effects of ocean acidification (Langdon et al., 2000; Doney et al., 2009; Andersson

and Gledhill, 2013; Shaw et al., 2015) because acidification makes it more difficult for

calcifying organisms to produce shells (Gattuso et al., 1999; Silverman et al., 2007). The

seawater chemistry in a coral reef ecosystem is naturally altered by organic production

and inorganic calcification resulting in large diel fluctuations in the seawater chemistry

(Ohde and Woesik, 1999; Bates et al., 2010; Shamberger et al., 2011; Gray et al., 2012).

In fact, reefs experience daily conditions that vary more widely than mean pre-industrial

to present pH conditions (Hofmann et al., 2011; Gray et al., 2012; Shaw et al., 2012;

Albright et al., 2013). Metabolism and calcification alter the water chemistry over the

reef, which are in turn controlled by light, temperature, water-mass movement, tides,

nutrient availability, community composition, and other physical parameters (Falter et al.,

2008, 2013; Anthony et al., 2013). The physical and biological drivers of this background

variability must be studied and understood in order to make projections on the

susceptibility of reef ecosystems to future changes in seawater chemistry due to ocean

acidification (Silverman et al., 2012; Falter et al., 2013; Albright et al., 2015; Shaw et al.,

2015).

Non-conservative A_T variability is primarily due to calcification (Fig. 4.1), and therefore A_T is a key indicator of reef NEC. Past calcification studies have been limited by the ability to measure calcification in situ on a temporal scale that captures the full range of variability. Studies have been conducted on smaller scales with mesocosm experiments (Gattuso et al., 1998; Andersson et al., 2009). *In situ* studies have been limited to shorter periods of time with one or two days of intense sampling (Falter et al., 2008; Shamberger et al., 2011), or with only a few samples per day e.g. every day at low tide for a month to capture one 24-hr diel cycle (Falter et al., 2008; Shamberger et al., 2011; Albright et al., 2015; Shaw et al., 2015). The 17-day A_T time series presented here provides unprecedented resolution of day and night calcification on the reef (Spaulding et al., 2014). The objectives of this study were to characterize the full range of CO_2 chemistry on the reef and to attempt to identify the primary controls of net ecosystem calcification by examining correlations between parameters. The relative importance of these drivers may be misunderstood in an in situ setting without high temporal resolution data, and resolving these drivers will be key in predicting the future of reef health in the world's oceans under changing conditions.
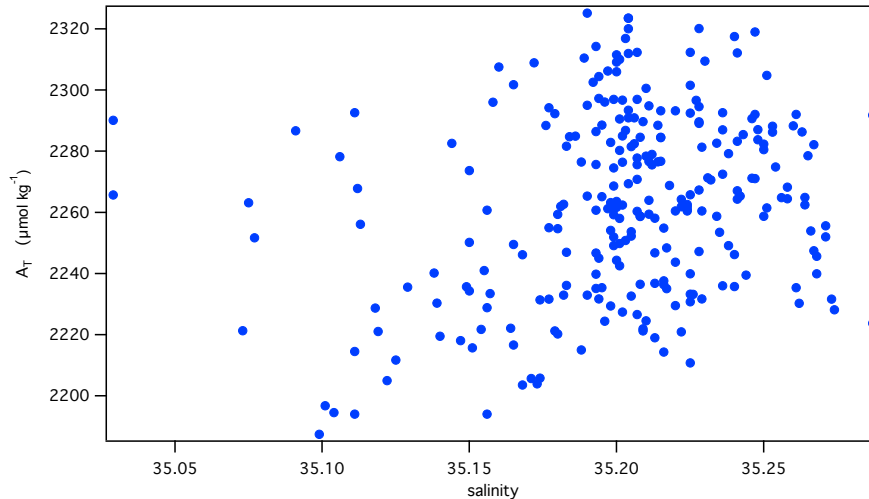
Figure 4:1 A_T plotted vs. salinity; there would be a clear trend if A_T were conservative with salinity as it is in the open ocean.

4.2 Results

4.2.1 Physical

The physical parameters are plotted in Figure 4.2, data sources are listed in Chapter 2. Water temperature varied only 3 °C during this study, from 23.9 – 27.0 °C and averaged 25.6 ± 0.7 (Fig. 4.2). The average salinity was 35.2 ± 0.04 (Fig. 4.2). There was no rainfall during this study. The daily tides ranged from 0.20 – 0.95 m. The predominantly northeast trade winds varied between 2.9 – 8.2 m s^{-1} with an average wind speed of 6.1 ± 0.9 m s^{-1}. Wind and wave height remained constant over the first several days of the deployment, and then increased to a maximum on June 13 before steadily decreasing to a minimum at the end of the time series.
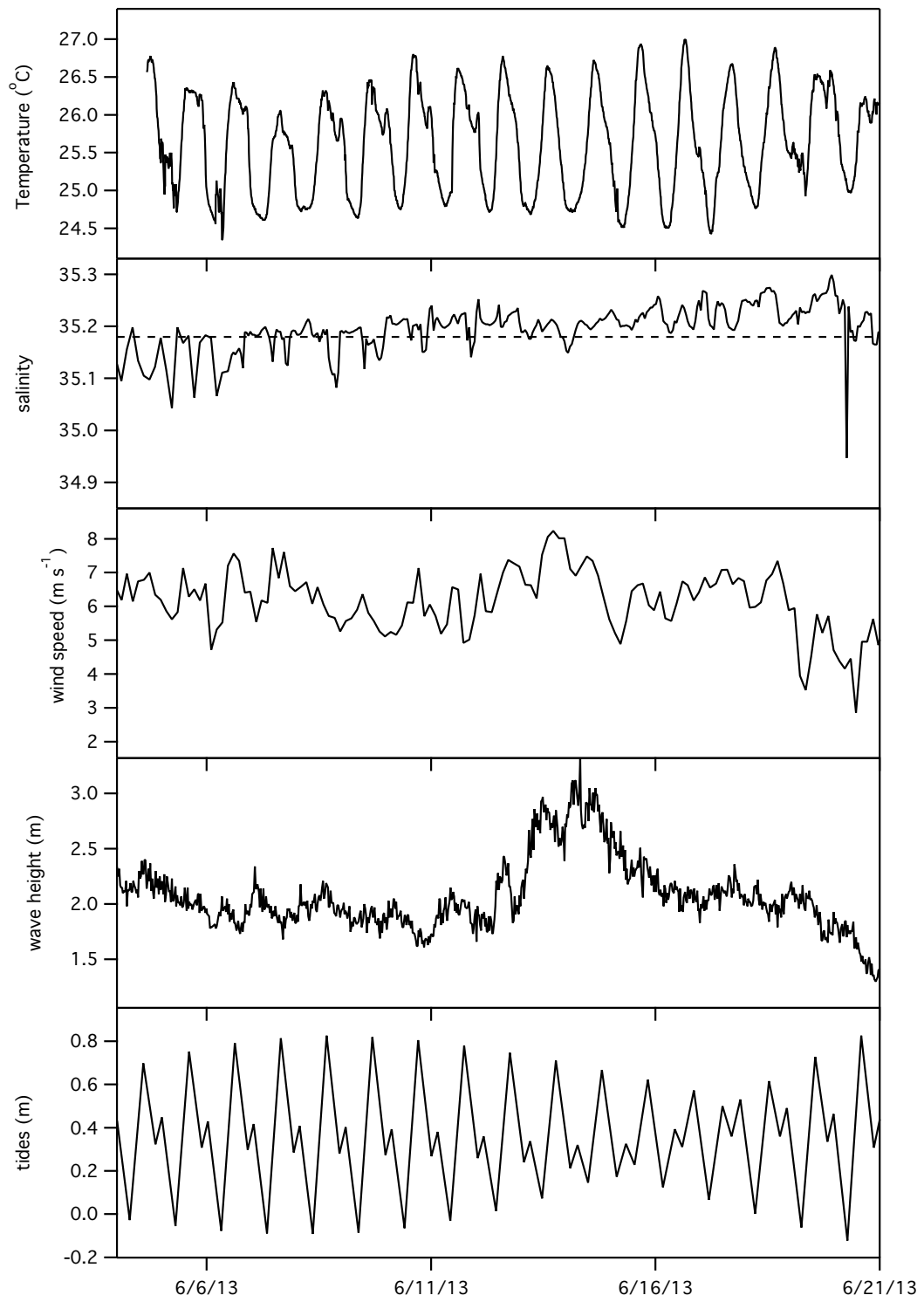
Figure 4:2 Temperature, salinity, wind speed, wave height and tides in Kaneohe Bay during this study. The dashed line represents the average HOT salinity.

4.2.2 Measured *in situ* trends

The diel water chemistry varied widely and is summarized in Table 4.1. The pH and pCO_2 mirrored each other, with pH reaching a minimum at dawn and a maximum in the afternoon around 2pm. DIC and Ω_{arag} also vary in opposition to each other; DIC is highest at dawn and Ω_{arag} is highest in the early afternoon, and vice versa (Fig. 4.3). Aragonite saturation states ranged from 2.33-4.71 and the peak magnitude varied day to day. Reports of mean Ω_{arag} for Kaneohe have varied widely from 2.84-3.62 (Kinsey, 1985; Shamberger et al., 2011); the mean Ω_{arag} from this study (3.22) falls within that range. The reef both increases and decreases the DIC from the open ocean source water (HOT); while the A_T on the reef is almost always lower than the source water A_T.

Table 4.1 Average values recorded over the study reported as mean ± standard deviation followed by the range. Asterisk (*) indicates measured parameters.

	mean ± SD	range
Temperature (°C)*	25.64 ± 0.69	23.9-27.0
Salinity*	35.2 ± 0.1	35.0-35.3
A_T (µmol kg^{-1})*	2263 ± 30	2187-2325
pH*	8.008 ± 0.084	7.847-8.218
DIC (µmol kg^{-1})	1978 ± 74	1823-2121
pCO_2 (µatm)	467 ± 90	291-672
Ω_{arag}	3.22 ± 0.53	2.33-4.71
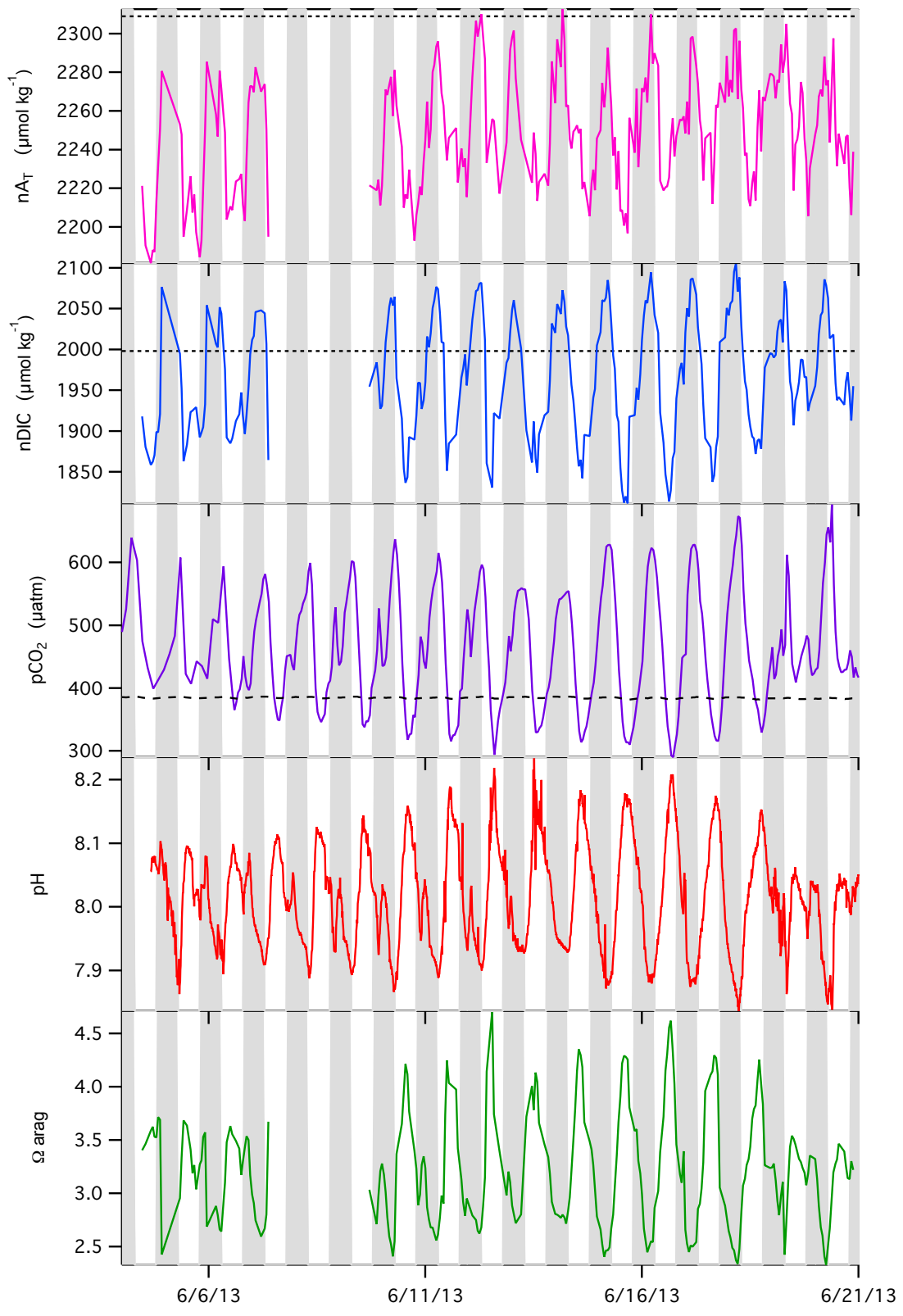
Figure 4:3 Salinity-normalized A_T (nA_T) from the SAMI-alk (pink) (dashed line represents average salinity-normalized HOT A_T), nDIC calculated from SAMI-alk – SAMI-pH (blue) (dashed line represents average salinity-normalized HOT DIC)**,** pCO_2 from the MAPCO2 (purple) (dashed line represents atmospheric pCO_2 from the MAPCO2)**,** pH from the SAMI-pH (red), and Ω_{arag} calculated from the SAMI-alk – SAMI-pH (green). Shaded bars represent nighttime.

There is a time-series trend in the maximum pH and the minimum pCO_2; pH maxima increase while pCO_2 minima steadily decline until June 15, and then pH maxima decrease through the rest of the study, while minima pCO_2 mirror this trend (Fig 4.3). This trend is also seen in the DIC and Ω_{arag}, but not in the A_T. There is no long-term trend in either the temperature or salinity. To show the pH and pCO_2 variability due to temperature, constant values for A_T and DIC were used with *in situ* temperature in CO2SYS to calculate pCO_2 and pH (Fig. 4.4). These results will be examined in the Discussion section below.
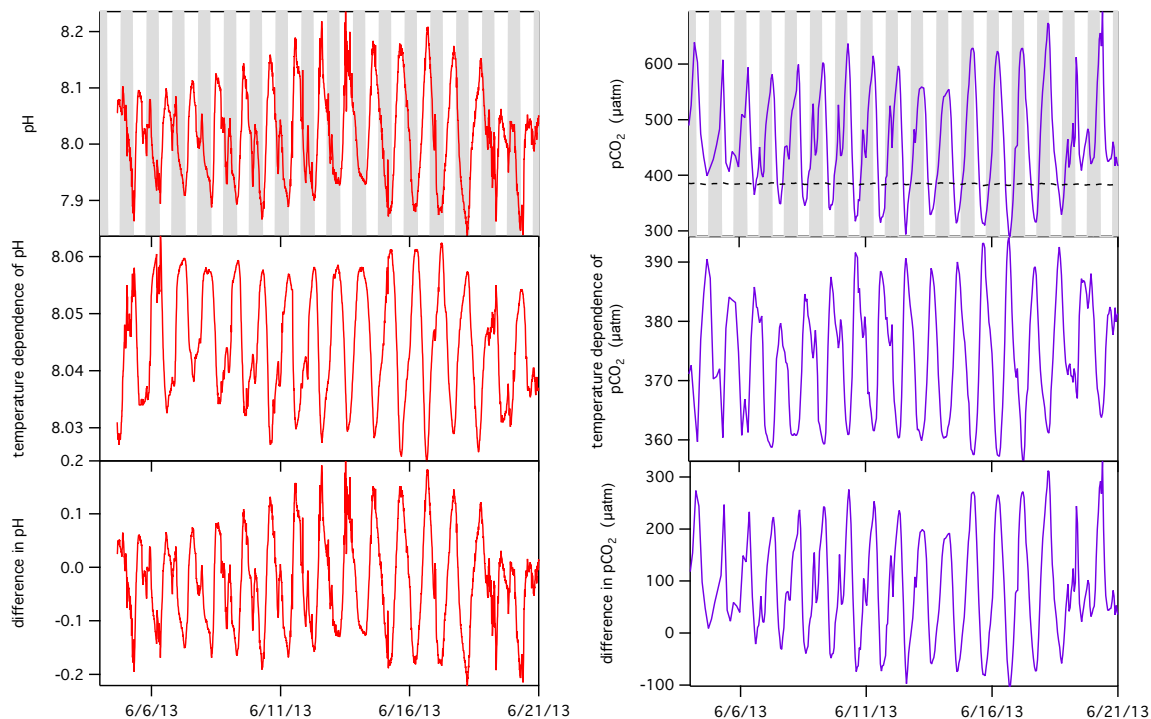
Figure 4:4 pH (red) and $p\mathrm{CO_2}$ (purple) measured *in situ* (top), calculated with *in situ* temperature and constant $\mathrm{A_T}$ and DIC (middle), and the difference (bottom) shows the temperature dependence of pH and $p\mathrm{CO_2}$ measurements.

4.2.3 Primary Production

Net ecosystem production (NEP) exhibits the same time series trend as pH, $p\mathrm{CO_2}$, and DIC (Fig. 4.3, Fig. 4.5). Photosynthesis and respiration nearly balanced each other daily; average integrated daytime NEP was 23 ± 11 mmol m^{-2} h^{-1} and average integrated nighttime NEP was -17 ± 7 mmol m^{-2} h^{-1}. Mean 24 hour NEP was 3.5 ± 5.7 mmol m^{-2} h^{-1}. Daytime values were defined as the integral of NEP when PAR > 0 and nighttime values were integrated when PAR = 0. The primary production to respiration ratio (P/R) for the reef was 1.2 ± 0.4, meaning the reef was net autotrophic. The average rate of gross

primary production (GPP, Eqn. 2.11) over the time series was 43.4 ± 18.3 mmol C m^{-2} d^{-1}, and the rate of community respiration (R) was 38.1 ± 18.8 mmol C m^{-2} d^{-1}.
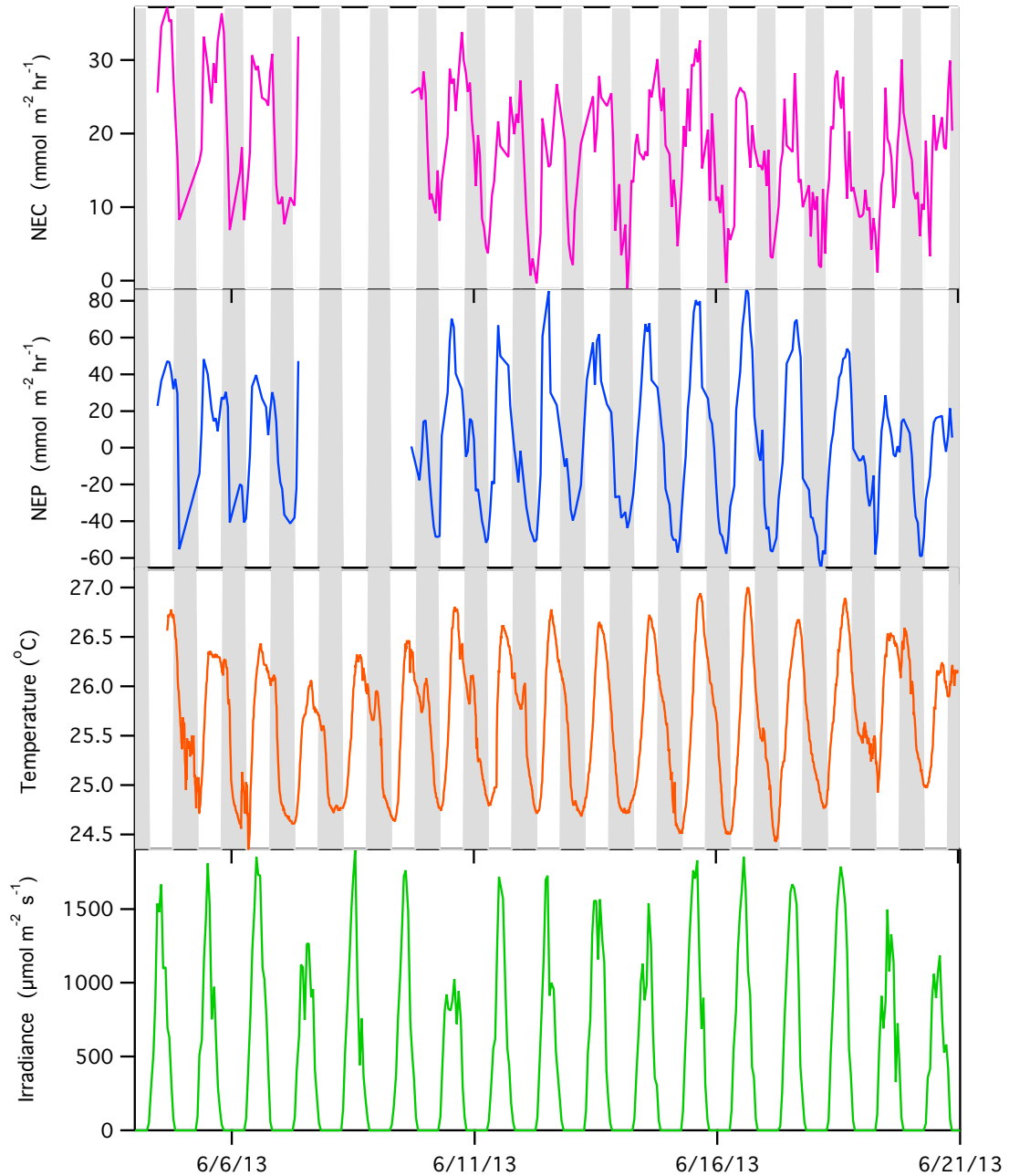
Figure 4:5 Time series of NEC (top), NEP (middle), and PAR (bottom).

Pearson's correlations (r) are presented in Table 4.2. NEP is correlated with NEC

with r = 0.73 (Table 4.2). NEP also has a better correlation with temperature (r = 0.91)

than PAR (r = 0.48), but the parameters used to calculate NEP (pH and $p\text{CO}_2$) are

temperature dependent.

Table 4.2 Correlations displayed as Pearson's r values all with p values < 0.05.
(n = 263 for each parameter)

	NEC	NEP
pH	0.60	0.98
Ω_{arag}	0.56	0.97
PAR	0.31	0.48
temperature	0.73	0.91
wind speed	0.30	0.42
$[\text{H}^+]$	0.63	0.99
NEC/NEP	0.73	0.73
tides	0.55	0.56

4.2.4 Net Ecosystem Calcification

A_T values below the HOT source water value of 2309 μmol/kg mean net

calcification was occurring, while values of A_T above the HOT A_T indicate net

dissolution. Three instances of net dissolution were measured on the reef, occurring as

single points on the nights of June 12, June 14, and June 16 (seen on figure 4.5 where

NEC dips below zero for one measurement on each of these days). Daytime NEC was

integrated when PAR > 0 and nighttime NEC was integrated when PAR = 0. With the

exception of these three points, the reef was always net calcifying with an average

integrated daytime NEC of 19 ± 3 mmol m^{-2} h^{-1} and an average nighttime NEC of 12 ± 3

mmol m^{-2} h^{-1}.

NEC is best correlated with NEP (r = 0.73) (Table 4.2). NEC is less correlated

with temperature (r = 0.73), and PAR (r = 0.31) than NEP. Like other studies (Ohde and

Woesik, 1999; Silverman et al., 2007; Andersson et al., 2009; Shamberger et al., 2011)

NEC is also correlated with Ω_{arag} (r = 0.56).

4.3 Discussion

4.3.1 Time-series trends

The following discussion will focus on June 10 – 20 where data from the entire

24-hour diel cycle were available (Fig. 4.3). Wind, waves, tides, and precipitation control

the physical properties of seawater in Kaneohe Bay (Smith and Key, 1975; Ringuet and

Mackenzie, 2005). Wave height and wind speed reached a maximum on June 14 and

decreased to a minimum at the end of the study, and the tidal range was the smallest from

June 14 – 19 (Fig. 4.2). Because of this decreased water movement, the average residence

time of 4 hours may have underestimated actual residence times on those days. The

largest tidal swings occurred during the last two days of the study, June 20-21, where the

4 hour average residence time may be an overestimation, thus dampening the NEP and

NEC signals. The tidal signal also shows up in the biogeochemical time series as a

shoulder particularly on days where the tidal range was small (Figs. 4.3 and 4.5, see small shoulder right at mark for June 11). Using an average residence time to calculate NEC and NEP smoothed this but did not eliminate it (Fig. 4.5). Additionally, all measured CO_2 system parameters and temperature were correlated with the tidal signal (e.g. daily high pH and temperature each corresponded to daily high tide, daily low pCO$_2$ corresponded to daily high tide, Table 4.2). This shows that the processes of NEP and NEC are sensitive to water movement driven by tides, but also that during this study high tide occurred on or near peak PAR and temperature each day.

The time series trend in pH, pCO$_2$, DIC, and hence NEP demonstrates that NEP is a primary driver of seawater chemistry on the reef. Calcification also significantly affects the seawater chemistry, resulting in diel A_T changes of up to 100 µmol kg^{-1}. The average ratio of NEP to NEC is 5:1 (Fig. 4.6). Because primary production rates are much larger than calcification rates, NEP is a more dominant control of seawater chemistry than calcification. This finding is consistent with studies conducted on other reef systems, (Shaw et al., 2012, 2015; McMahon et al., 2013; Albright et al., 2015) and mesocosm studies (Gattuso et al., 1998; Langdon and Atkinson, 2005; Langdon et al., 2003).
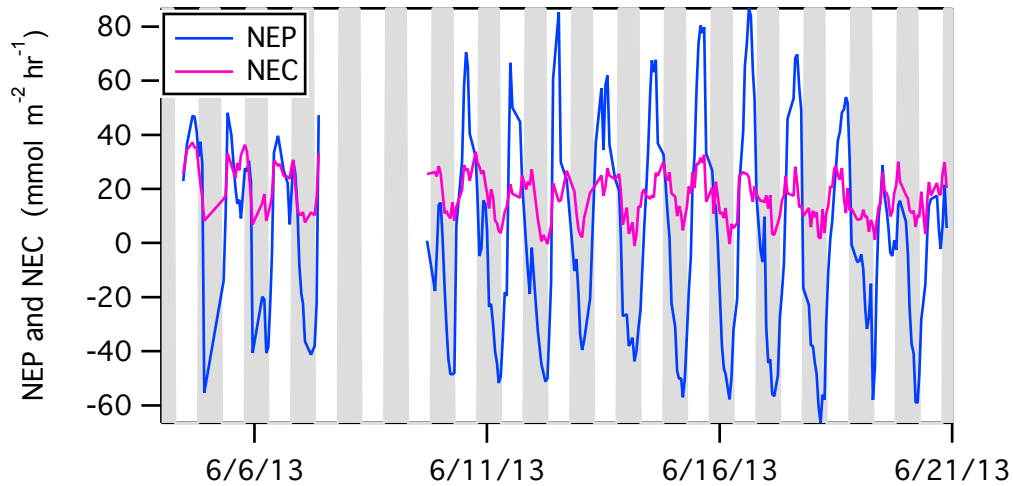
Figure 4:6 NEP (blue) and NEC (pink) plotted on the same scale. Data from Figure 4.5.

NEP is the parameter best correlated to NEC (Table 4.2), supporting that the strongest driver of calcification on the reef is NEP. In an attempt to see if observed net ecosystem production could predict NEC, a linear regression of NEC as a function of NEP was determined (Eqn. 1).

$$NEC = (16.9 \pm 0.4 \text{ mmol CaCO}_3 \text{ m}^{-2} \text{ h}^{-1}) + (0.17 \pm 0.01 \frac{\text{mmol CaCO}_3 \text{ m}^{-2} \text{ h}^{-1}}{\text{mmol C m}^{-2} \text{ h}^{-1}}) \bullet NEP \qquad (4.1)$$

This equation explains 54% of the variance in NEC. A correlation between and NEC and Ω_{arag} has been reported in Kaneohe Bay (Shamberger et. al., 2011), and on other reefs (McMahon et al., 2013; Shaw et al., 2015; Decarlo et al., 2017), so Ω_{arag} is included on the plot of NEC and predicted NEC from Eqn. 1 in Figure 4.7. If Ω_{arag} were an important factor in explaining diel calcification, NEC would be greater than predicted by Eqn. 4.1 at high Ω_{arag} and less than predicted by Eqn. 4.1 when Ω_{arag} is low. Figure 4.7 shows that

this is not the case, predicted NEC is both higher and lower than observed NEC at high values of $\Omega_{arag.}$ The predicted NEC also differs from observed NEC on days when NEC and NEP are decoupled from each other and peak PAR (e.g. June 11) and when observed daytime peak NEP was low, but NEC remained high (e.g. June 19-20).
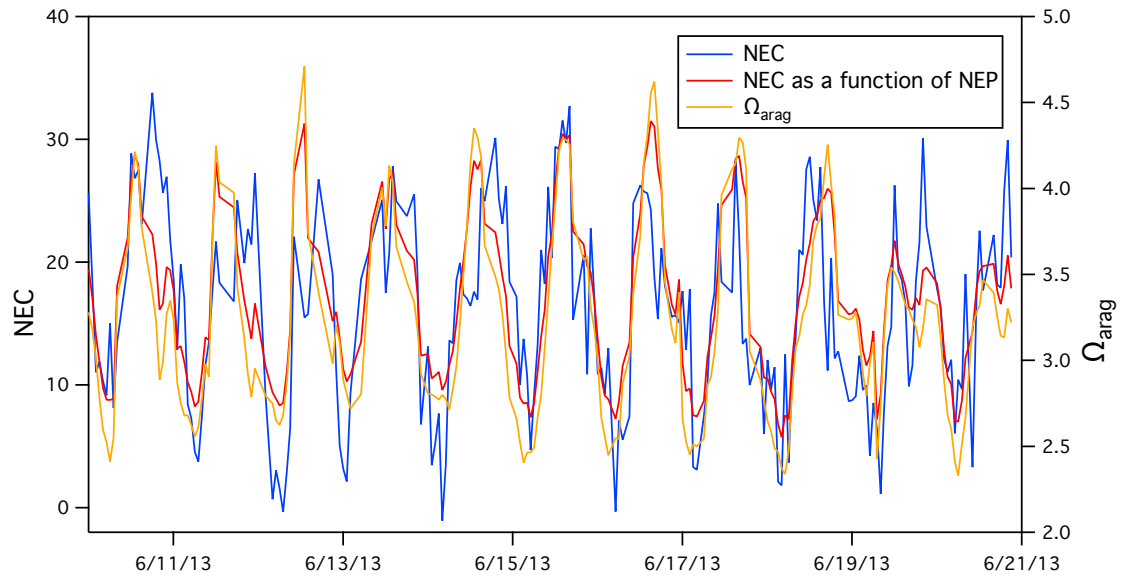
Figure 4:7 Measured NEC (mmol m^{-2} h^{-1}) (blue) shown with NEC predicted from Eqn. 4.1 (red) on left axis, and Ω_{arag} on right axis.

Additionally, NEP and NEC are decoupled on hourly time scales (Fig. 4.8) throughout the study. This phenomenon has been observed before both in Kaneohe Bay (Shamberger et al., 2011) and elsewhere (Falter et al., 2012) where for example peak NEC and NEP will occur at the same time some days, and several hours apart on others (Fig. 4.8). The mechanism for this decoupling of NEP, NEC and peak PAR cannot be explicitly isolated at present; these decoupling events are not correlated any other mean

parameter (e.g. average daily PAR, peak PAR, temperature, tides). It may be that the reef

is calcifying above some threshold where diel NEC is not directly affected by diel

variability in NEP and PAR; this is the first example of this from this data set, but more

will be discussed in the following sections. This is an example of where long-term high

temporal resolution records are necessary to determine how frequent or infrequent these

decoupling events are in a coral reef environment.
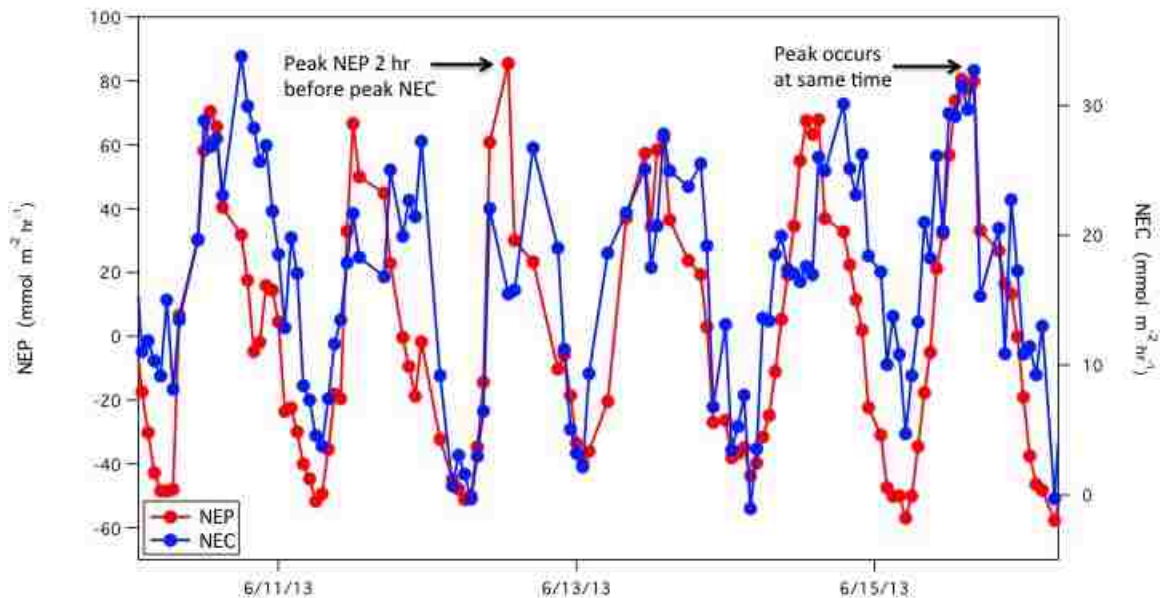
Figure 4:8 72 hours of NEP (red) and NEC (blue) demonstrating phase coherence and short-term decoupling.

4.3.2 Controls of diel variability

There are chemical feedbacks between NEC and NEP that potentially contribute

to their high correlation. The formation of $CaCO_3$ by NEC produces CO_2, which is

consumed by photosynthesis. NEC and NEP are linked because the products of one are

the reactants of the other. Additionally, in any *in situ* coral reef study a number of

parameters that can affect NEC and NEP covary, *e.g.* light, temperature, currents, diel

winds, Ω_{arag}, and nutrient availability. The linear regression model (Fig. 4.7) explains the

phase of NEC (highest rates occur during the day, rates decline at night), but not

necessarily the absolute rate of calcification. Average daily calcification rates vary by

16% (19 ± 3 mmol m^{-2} h^{-1}) from day to day, while average daily NEP varies by 50% (23

± 11 mmol m^{-2} h^{-1}) during the study (Fig. 4.9). The changes in NEP amplitude do not

show a corresponding change in NEC amplitude. The last two days of the study, for

example, have much lower daytime integrated rates of NEP; in fact there is daytime net

respiration on June 19. Yet, daily-integrated rates of NEC over those two days are within

± 3 mmol m^{-2} h^{-1} of the average daily NEC (Fig. 4.9), and integrated PAR on June 18 is a

daily maximum for the study. There is no correlation between daily-integrated NEC or

NEP and PAR, thus daily light availability is not a good predictor for daily rates of NEC

or NEP.
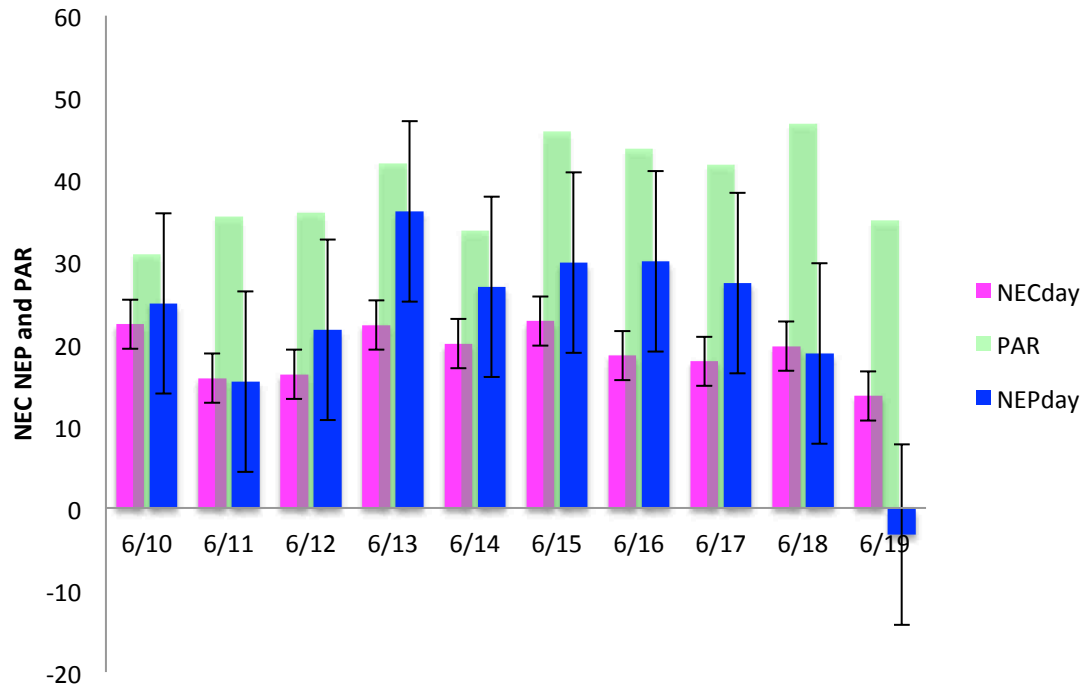
Figure 4:9 Daytime integrated ΣNEP and ΣNEC (mmol m^{-2} h^{-1}) defined as the area under the curve of NEP or NEC when PAR > 0, and daily integrated ΣPAR (mol photons m^{-2} d^{-1}) shown on days where the full diel cycle was measured for NEP and NEC. Error bars indicate standard deviations.

Both exponential and linear relationships between light and NEP (exponential) or NEC (exponential and linear) on coral reefs have been established in previous studies (Gattuso et al., 1996; Falter et al., 2012; Albright et al., 2013; Takeshita et al., 2016). However, in this study there are low correlation coefficients between NEP and PAR (r = 0.48) and NEC and PAR (r = 0.31) during this study (Table 4.2). Hourly binned NEP and NEC rates (the same hour each day was averaged) are plotted with daily-integrated PAR in Figure 4.10. The composite plot also includes all measured data (Fig. 4.5). Instead of the expected exponential relationship, a diel hysteresis emerged where the morning NEP rates are lower than afternoon NEP rates at similar PAR. The hysteresis suggests that there is another variable not accounted for in the NEP – PAR relationship. It could be in

69

part a result from the offset of peak PAR and peak NEP in Kaneohe Bay, but is likely a

signal in the residence time of the water from the diel tides. It demonstrates that caution

should be used when applying a previously established exponential relationship between

NEP and PAR in order to predict NEP, especially because wide variability has been

shown between reefs (Albright et al., 2013; Takeshita et al., 2016), and seasonally on the

same reef (Falter et al., 2012).
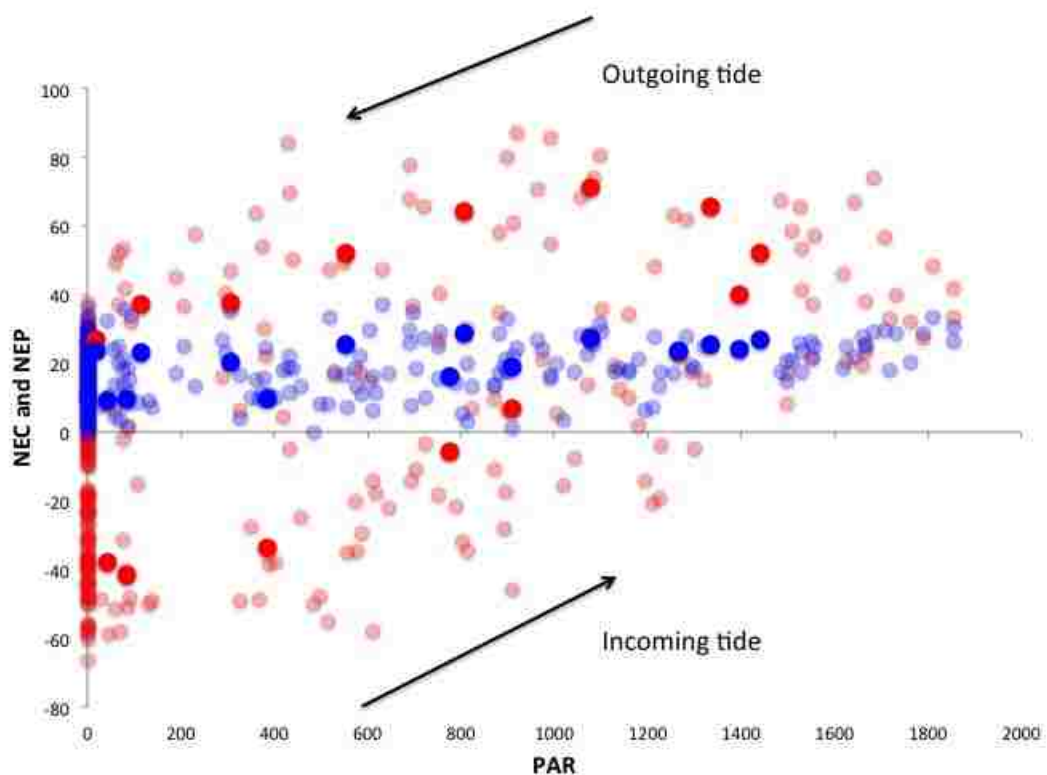
Figure 4:10 NEC (blue, mmol m^{-2} hr^{-1}) and NEP (red, mmol m^{-2} hr^{-1}) vs. PAR (μmol photons m^{-2} s^{-1}). Individual measurements shown in shaded circles, hourly binned averages shown in solid circles.

It could also be that in Kaneohe Bay, morning production must overcome a night

of net respiration; production is lower in the morning because it is transitioning from 12

hours of net respiration. Whereas, late afternoon production, at the same PAR as morning production, follows hours of higher rates of net production. Unlike NEP, net calcification continues throughout the hours of zero PAR; average integrated nighttime NEC is 12 ± 3 mmol m^{-2} h^{-1}. NEC rates are high enough to draw down Ω_{arag} if they were the only process occurring (absent NEP). Instead high Ω_{arag} values were observed at high NEC rates because production sustains the high Ω_{arag} by consuming CO_2 and producing CO_3^{2-} (Fig. 4.11). At night during net respiration, net dissolution was only observed for three measurements all corresponding to NEP rates between -40 to -60 mmol m^{-2} h^{-1}. A similar threshold has been observed on other reefs, where NEC crosses from net calcification to net dissolution at high rates of net respiration. This same threshold of NEC = 0 at NEP of -50 mmol m^{-2} h^{-1} was observed on the Dongsha Atoll, northern South China Sea in June 2014 (Decarlo et al., 2017), -25 mmol m^{-2} h^{-1} in the winter and -50 mmol m^{-2} h^{-1} in the summer on the Davies Reef flat in the central Great Barrier Reef, (Albright et al., 2013) and NEP values between 0 mmol m^{-2} h^{-1} and -20 mmol m^{-2} h^{-1} on Heron Island and One Tree Island Great Barrier Reef (Shaw et al., 2015; McMahon et al., 2018). Though the point of intersection varies between reefs and seasons, there is some consistency with very similar thresholds observed from widely different locations.
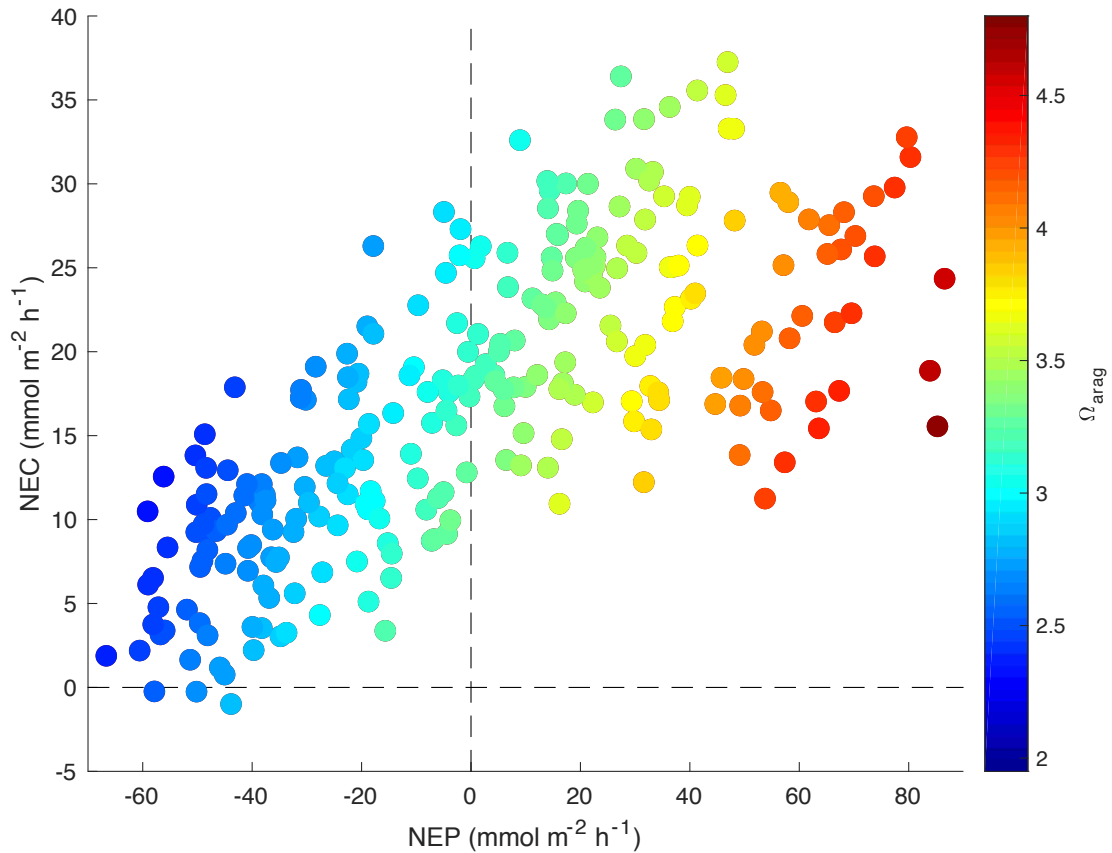
Figure 4:11 Relationship between Net Ecosystem Calcification (NEC) and Net Ecosystem Production (NEP). Points shaded with Ω_{arag} (colorbar). Horizontal dashed line represents net calcification (above) and net dissolution (below), vertical dashed line represents net production (right) and net respiration (left).

NEC appears to be at some threshold where calcification rates on the reef are not affected by small, short-term changes in NEP. This could be explained if heterotrophic processes are a greater influence on calcification than autotrophic processes in Kaneohe Bay especially at night. The stability in NEC even when there are changes in NEP, light, and currents also supports model and incubation studies that conclude that marine corals affect carbonate chemistry at the site of calcification to produce internal conditions that are more favorable for calcification than those of the surrounding water (McCulloch et al., 2012; Venti et al., 2014; Cyronak et al., 2016).

4.3.3 A_T – DIC relationship

The diel changes in DIC and A_T measured directly at CRIMP-2 can also be used
to examine community metabolism without quantifying residence times. A Deffeyes
diagram (Deffeyes, 1965) plotted in Figure 4.12 shows the relative ratio of calcification
to photosynthesis. Here the A_T – DIC relationship is used to explore the extent to which
benthic community carbon fluxes alter the aragonite saturation state of the overlying
water (Deffeyes, 1965; Suzuki and Kawahata, 2003; Andersson and Gledhill, 2013). The
theoretical effects of photosynthesis – respiration, gas exchange, and calcification –
dissolution are plotted as vectors. One mole of DIC is consumed for every mole of
organic carbon produced through photosynthesis while A_T is negligibly affected. For
every mole of $CaCO_3$ produced by calcification, A_T decreases by 2 moles and DIC
decreases by 1 mole. Hence, The theoretical calcification vector has a slope of two
(Suzuki and Kawahata, 2003). Air – sea CO_2 flux affects the DIC, but not the A_T, shifting
the midpoint of the A_T-DIC line horizontally. Lines of constant Ω_{arag} are shown as
colored isopleths The observed A_T – DIC slope of 0.33 corresponds to the higher rates of
NEP than NEC seen in this study (NEP:NEC = 5:1), further supporting that NEP is a
more dominant control of the water chemistry than calcification. Here the A_T – DIC
relationship crosses the Ω_{arag} isopleths (the slope of the A_T-DIC best fit line is less than
the Ω_{arag} isopleths) meaning that biological production drives an increase in the saturation
state during the day, allowing for high rates of NEC.
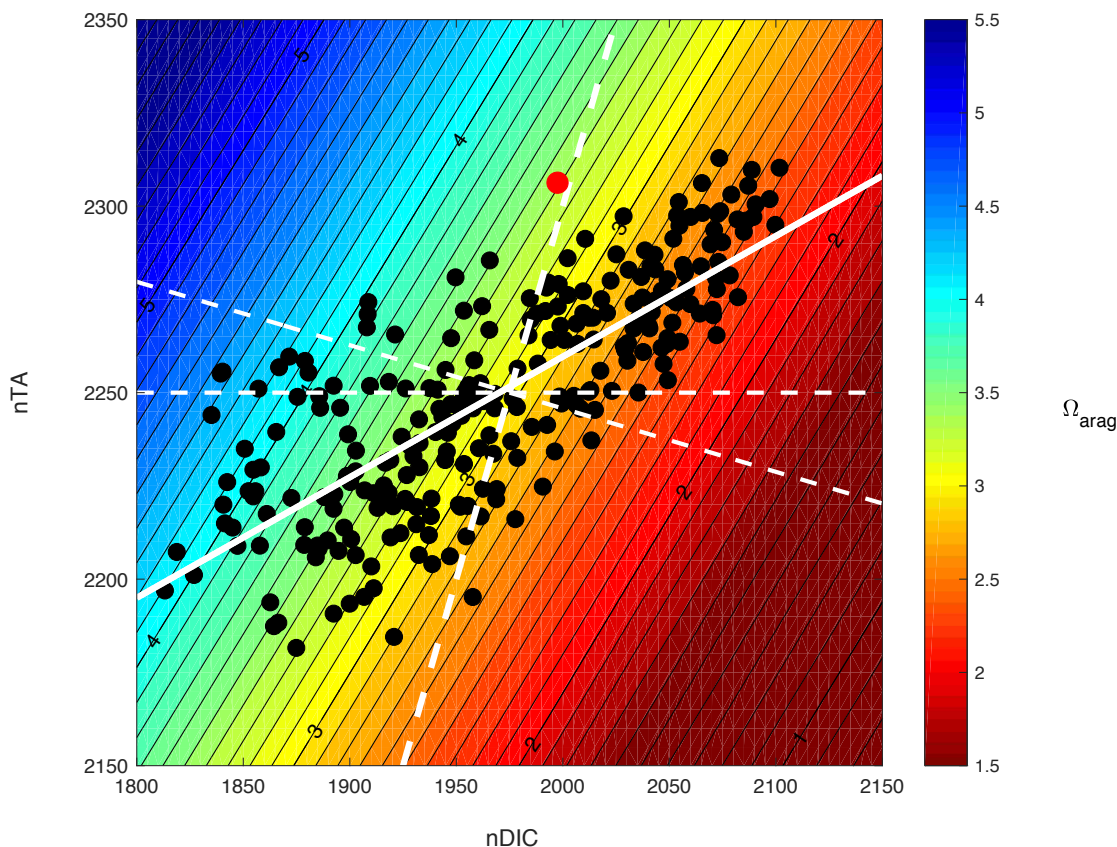
Figure 4:12 Salinity normalized A_T versus DIC (µmol kg^{-1}), data from Figure 4.3, where black data points are time series data from the reef. The linear-least squares best-fit line (solid white) has a slope of 0.33. The red dot represents open ocean source water from HOT. Vectors representing calcification – dissolution (slope of 2:1), photosynthesis – respiration (Redfield ratio), and gas exchange (horizontal) are shown as dashed lines. Colors correspond to Ω_{arag}.

During this study, the A_T – DIC slope varied daily from $0.21 - 0.48$ (Fig. 4.13) an observation that has not been reported in other studies on this reef (Falter et al., 2011; Shamberger et al., 2011; Drupp et al., 2013) or on other reefs (Gattuso et al., 1998; Albright et al., 2013, 2015; Lantz et al., 2013; McMahon et al., 2013). Figure 4.13 shows the two daily extremes of the A_T – DIC slope. Establishing a baseline A_T – DIC relationship can serve as a ruler for how future ocean conditions may perturb the NEC –

NEP balance, however, the slope of the daily A_T – DIC relationship is not correlated with

daily-integrated PAR.
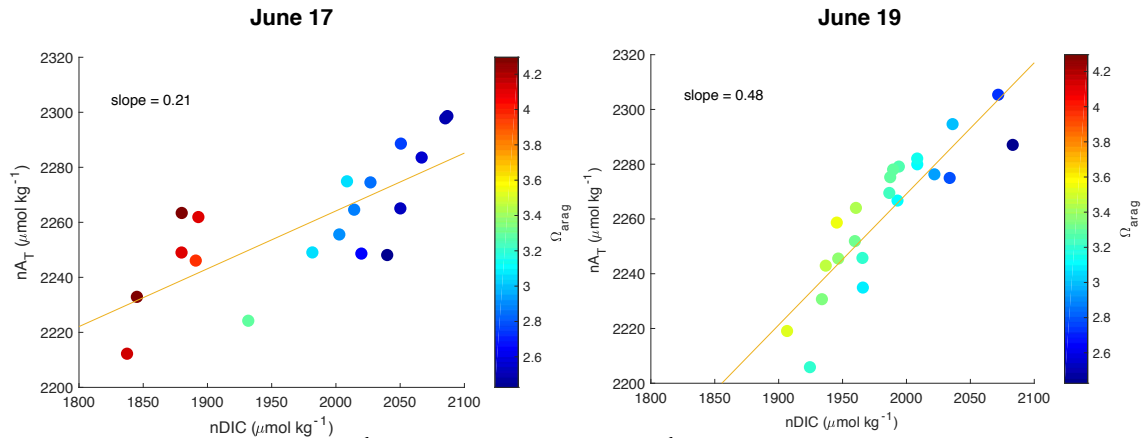
Figure 4:13 nDIC (µmol kg^{-1}) versus nA$_T$ (µmol kg^{-1}) plots for June 17 and June 19. Measured points are colored with Ω_{arag}. Lines represent a linear fit through the data with the slope shown.

Unlike studies on other reefs (Suzuki and Kawahata, 2003; Andersson and

Gledhill, 2013) where it was found that reefs decreased DIC from the source water, here

the reef almost always decreased A_T from the open ocean source (HOT), but both

increases and decreases the DIC (Fig. 4.12). DIC values significantly higher than the

HOT value mean net respiration. An A_T – DIC slope of 1.1 corresponds to the previously

discussed threshold values of NEC = 0 mmol m^{-2} hr^{-1} and NEP = -50 mmol m^{-2} hr^{-1} using

the same values for source water A_T and DIC (HOT) and residence time (4 hr) that were

used in this study. The days during this study with a higher A_T – DIC slopes (e.g. June

19, Fig. 4.13) also corresponded to lower observed values of Ω_{arag}. Consequently, as the

measured ratio of A_T – DIC approaches 1 on this reef, and potentially others, the reef

may change over from net calcifying to net dissolving.

4.3.4 Other Kaneohe Bay studies

This study found the reef in Kaneohe Bay to be net autotrophic, with a primary production-to-respiration ratio (P/R) of 1.2 ± 0.4. Falter et al. (2011) reported a P/R of 1.04 during October 2006 in Kaneohe Bay. The magnitudes of NEP above and below zero in this time series are similar, further illustrating that most carbon fixed during the day is rapidly metabolized at night, and that increases in production drive increases in respiration. R is correlated with P ($r^2 = 0.67$), and this study displayed a similar short-term coherence between P and R as that seen in the Falter's October 2006 data (Falter et al., 2011). Unlike Falter et al., (2011), daily integrated P during this study does not vary linearly with daily integrated PAR ($r^2 = 0.1$).

Table 4.3 Comparison of average daily values of temperature, salinity, Ω_{arag}, pCO_2, NEC and NEP of four studies conducted in Kaneohe Bay.

Kaneohe Bay	Temp (°C)	Salinity	Ω_{arag}	pCO_2 (µatm)	NEC (mmol m^{-2} h^{-1})	NEP (mmol m^{-2} h^{-1})	Study
Winter	24.6	35.0	3.26	325	9.0	-3.1	Kinsey, 1985
Summer	27.1	34.9	3.62	328	11.4	-14.2	Kinsey, 1985
Winter	23.4	34.9	2.84	392	12.2	-2.3	Shamber et al., 2011
Summer	26.3	35.2	2.86	394	9.8	-6.6	Shamber et al., 2011
Summer	25.6	35.2	3.22	398	16.3	3.5	This study

Average daily summertime NEC rates reported during the summer of 1970 in Kaneohe Bay were 11.4 mmol m^{-2} h^{-1} (Kinsey, 1985). A 48-hr study at CRIMP-2 conducted in 2011 measured lower average daily NEC (9.8 mmol m^{-2} h^{-1}) in the summer, but a higher rate of NEC during the winter (12.2 mmol m^{-2} h^{-1}) (Shamberger et al., 2011). Average daily NEC during this study was higher than both (16.3 ± 2.4 mmol m^{-2} h^{-1}). The atmospheric pCO$_2$ in 1970 was substantially lower than the pCO$_2$ today, 328 ppm and 398 ppm respectively (Table 4.3). The average Ω_{arag} was higher in 1970 than in 2011 (3.61 and 2.86, respectively), but Ω_{arag} measured during this study fell between these values. The relatively high, steady rates of NEC measured could imply the robustness of calcifiers in Kaneohe Bay even under drastically different CO$_2$ system conditions. By contrast, NEC rates have reduced by ~44% over the same time period on One Tree Island reef on the Australian coast (Silverman et al., 2012; Albright et al., 2013). But as we have shown, there are many factors that affect NEC and no direct connection between atmospheric pCO$_2$ and NEC can be drawn from these three isolated studies. High rates of nutrient uptake like those observed in Kaneohe (Falter et al., 2004) can reduce sensitivity of NEC to changes in aragonite saturation state (Silverman et al., 2007). A concurrent increased presence of H$^+$ from ocean acidification could result in a larger proton gradient at the site of calcification against which calcifiers must contend (Roleda et al., 2012). NEC is correlated with H$^+$ ($r = 0.63$, Table 4.2), but as the reef was always net calcifying during this study, this is likely not significantly affecting calcification rates.

4.4 Conclusions

The SAMI-alk allowed autonomous characterization of diel A_T for 17 days on a coral reef in Kaneohe Bay (Spaulding et al., 2014). The study demonstrated the SAMI-alk is an important tool for characterizing calcification and improving our understanding of the controlling biogeochemical processes *in situ*. Using the SAMI-alk in targeted studies on reef calcification and metabolism will aid in assessing the potential future impacts of ocean acidification on coral reefs. The A_T – DIC relationship has previously been used as a baseline for reefs (Andersson and Gledhill, 2013) (Fig. 4.12), but high resolution data from this study show that it can change daily (Fig. 3.13). While there is a relationship between production, calcification, and light, they decouple from day to day (Fig. 4.8), and from morning to afternoon (Fig. 4.10). Daily-integrated PAR does not predict high daily-integrated rates of NEP or NEC (Fig. 4.9). These differences would not have been observed without the high temporal resolution of the SAMI-alk.

The natural trends in carbonate chemistry in Kaneohe Bay vary widely over diel cycles. NEP, and to a lesser extent NEC, controlled the seawater chemistry. A strong relationship between NEC and NEP was observed, suggesting that production drives NEC, although it is not the only parameter necessary for calcification as high rates of NEC were observed on days with low productivity (Figs 4.6 and 4.9). Because so many factors influencing NEP and NEC covary, no relationship between only two factors (*e.g.* PAR, Ω_{arag}, NEP, NEC) completely explained the observed variability. The natural diel variability of NEC in Kaneohe Bay is greater in magnitude than predicted changes in NEC due to ocean acidification (Langdon et al., 2000; Shaw et al., 2015) mean levels will

change and they might regulate everything. Anthropogenic changes may be lost in the noise of this natural variability unless the natural variability is well characterized. Additional long-term studies using the SAMI-alk could establish more robust relationships for the biogeochemistry on coral reefs.

Chapter 5

Summary and Future Work

5.1 Summary

Over 250 individual A_T measurements were made during the first deployment of the autonomous instrument for alkalinity, the SAMI-alk between June 4, 2013 and June 21, 2013. This allowed us to capture the full diel variability during the 17-day time series (Fig. 4.3). Additional continuous measurements of pH, and pCO_2 made during the study were used in the analysis of the seawater CO_2 system in Kaneohe Bay. The composite data set is the most comprehensive continuous evaluation of the biogeochemistry on a coral reef.

The SAMI-alk was deployed with a SAMI-pH on the CRIMP-2 buoy in Kaneohe Bay with an existing MAPCO2 system, SeaFET (pH) and Sea Bird CTD. The main focus of this deployment was to assess the ability of the SAMI-alk to autonomously measure A_T *in situ* in a highly variable environment. Discrete samples were taken throughout the study and analyzed for A_T to determine the accuracy of the SAMI-alk as -1.6 ± 15.7 μmol kg soln^{-1}. The objectives of this research, as presented in the previous chapters, were to 1) evaluate the internal consistency of the CO_2 system using three in situ parameters (pCO_2, pH, and A_T); and 2) use the A_T data to assess the relationship between coral production and environmental conditions.

The seawater CO_2 system in Kaneohe Bay was fully characterized four ways (Fig. 3.2) during the study using the combination of the SAMI-alk with (1) a SAMI-pH, (2) a SeaFET (pH), and (3) a MAPCO2 system, and (4) with the pH- pCO_2 combination (Fig. 3.3) from the SAMI-pH and MAPCO2 to do the equilibrium calculations. This gave us

another way to evaluate the performance of each instrument individually and compare the possible combinations. The SAMI-pH measured more frequently and has the highest reported accuracy of the pH sensors. Both pH sensors agreed to within 0.006 ± 0.022 pH units (Table 3.5), but the SeaFET fouled seven days into the study, and required an offset to correct the data post deployment (Fig. 3.1). The pCO_2 time series decoupled with the two calculated pCO_2 data sets at low values of pCO_2 when the seawater pCO_2 changed from decreasing to increasing each day (Fig. 3.11). This systematic error propagated through the equilibrium calculations, and is likely a design issue specific to the equilibration that takes place during each measurement in the MAPCO2 system. For these reasons we determined that the SAMI-pH – SAMI-alk combination for calculating CO_2 system equilibria was the most robust and therefore used it in the rest of our analysis (Fig. 4.3).

Kaneohe Bay experiences dynamic pH, pCO_2, DIC, and A_T fluctuations each day (Fig. 4.3). Production and respiration decrease and increase the DIC, respectively, from the open ocean source water, resulting in daily pH changes of ~0.1 pH units. Calcification draws down the source water A_T. The pCO_2 is altered by both biology and gas flux, as its range is both below (291 µatm) and above (672 µatm) atmospheric pCO_2 (398 µatm). Net ecosystem production and net ecosystem calcification were evaluated as the most significant drivers of seawater chemistry on the coral reef. Both processes varied greatly in their contribution to the diel cycles of inorganic carbon. Time series trends in pH, pCO_2 and DIC and NEP demonstrate the role of NEP in governing the water chemistry on the reef (Fig. 4.3). We determined that NEP is a significant driver of NEC; they are correlated and a linear regression model explains 54% of the variance (Fig. 4.7).

The correlation of NEC with NEP (Table 4.2), and hence the factors that govern NEP such as light, explains the phase of NEC, but not the absolute rates. High rates of calcification were observed on days where NEP was relatively low (Fig. 4.5), and NEC and NEP became de-coupled on an hourly interval nearly every day (Fig. 4.8). While PAR appears to control NEP as expected, it does not follow the established tangential relationship shown on other reefs (Fig. 4.10), and there is no relationship between NEC and PAR (Fig. 4.9). The observed correlations and de-coupling also suggest that the reef is at a threshold of calcification that it can sustain through day-to-day changes in production and light availability. Moreover, when NEP dropped to approximately -50 mmol m^{-2} h^{-1}, NEC switched from net calcification to net dissolution (Fig. 4.11). This appears to be an important threshold for sustaining coral growth, and has been shown on other reefs (Albright et al., 2013; Shaw et al., 2015; Decarlo et al., 2018; McMahon et al., 2018).

The A_T-DIC relationship (Fig. 4.12) represents direct measurements made during this study, rather than calculations of NEC and NEP that must account for water mass movement, and supports these conclusions because it too varies from day to day (Fig. 4.13). Previous observations made in Kaneohe Bay (Falter et al., 2011; Shamberger et al., 2011) and on other reefs (Shaw et al., 2015; Albright et al., 2018; McMahon et al., 2018) additionally demonstrate the dramatic range of water chemistry that coral reefs experience. Our conclusions are consistent with others that the controls of reef biogeochemistry are highly variable both daily and seasonally, and are individual to each reef ecosystem.

5.2 Future Work

The SAMI-alk autonomously measured A_T for the first time during this study; additional SAMI-alk sensors should be built and put through extensive field testing to further establish confidence in the reliability of the SAMI-alk and the quality of the A_T data. More deployments of the SAMI-alk will also be key in evaluating the long-term accuracy of the sensor. Preliminary work by Adam Prody (UM DeGrandpre lab) has shown promising results of the reproducibility of three SAMI-alk sensors in a controlled seawater test tank. These SAMI-alk sensors have since been deployed on a coral reef in Bermuda. Continued coral reef studies would ideally be conducted with the sensors in different coral cover and biological environments on the same reef to better evaluate the effects of NEP on NEC variability. This work should also include off-reef sampling during the study on carefully defined transects to better characterize the end-member waters and the residence times of the waters affected by reef calcification and production.

References

Albright, R.; Langdon, C.; Anthony, K. R. N. Dynamics of Seawater Carbonate Chemistry, Production, and Calcification of a Coral Reef Flat, Central Great Barrier Reef. *Biogeosciences* **2013**, *10* (10), 6747–6758.

Albright, R.; Benthuysen, J.; Cantin, N.; Caldeira, K.; Anthony, K. Coral Reef Metabolism and Carbon Chemistry Dynamics of a Coral Reef Flat. *Geophys. Res. Lett.* **2015**, *42* (10), 3980–3988.

Albright, R.; Takeshita, Y.; Koweek, D. A.; Ninokawa, A.; Wolfe, K.; Rivlin, T.; Nebuchina, Y.; Young, J.; Caldeira, K. Carbon Dioxide Addition to Coral Reef Waters Suppresses Net Community Calcification. *Nature* **2018**, *555* (7697), 516–519.

Andersson, a. J.; Kuffner, I. B.; Mackenzie, F. T.; Jokiel, P. L.; Rodgers, K. S.; Tan, a. Net Loss of $CaCO_3$ from a Subtropical Calcifying Community Due to Seawater Acidification: Mesocosm-Scale Experimental Evidence. *Biogeosciences* **2009**, *6* (8), 1811–1823.

Andersson, A. J.; Gledhill, D. Ocean Acidification and Coral Reefs: Effects on Breakdown, Dissolution, and Net Ecosystem Calcification. *Ann. Rev. Mar. Sci.* **2013**, *5*, 321–348.

Andersson, A. J.; Mackenzie, F. T.; Lerman, A. COASTAL OCEAN AND CARBONATE SYSTEMS IN THE HIGH CO 2 WORLD OF THE ANTHROPOCENE. *Am. J. Sci.* **2005**, *305* (November), 875–918.

Anthony, K. R. N.; Diaz-Pulido, G.; Verlinden, N.; Tilbrook, B.; Andersson, a. J. Benthic Buffers and Boosters of Ocean Acidification on Coral Reefs. *Biogeosciences* **2013**, *10* (7), 4897–4909.

Bandstra, L.; Hales, B.; Takahashi, T. High-Frequency Measurements of Total CO2: Method Development and First Oceanographic Observations. *Mar. Chem.* **2006**, *100* (1–2), 24–38.

Bates, N. R.; Amat, a.; Andersson, a. J. Feedbacks and Responses of Coral Calcification on the Bermuda Reef System to Seasonal Changes in Biological Processes and Ocean Acidification. *Biogeosciences* **2010**, *7* (8), 2509–2530.

Bates, N. R.; Astor, Y. M.; Church, M. J.; Currie, K.; Dore, J. E.; González-Dávila, M.; Lorenzoni, L.; Muller-Karger, F.; Olafsson, J.; Santana-Casiano, J. M. A Time-Series View of Changing Ocean Chemistry Due to Ocean Uptake of Anthropogenic CO2 and Ocean Acidification. *Oceanography* **2014**, *27* (1), 126–141.

Breland, J. A.; Byrne, R. H. Spectrophotometric Procedures for Determination of Sea Water Alkalinity Using Bromocresol Green. *Deep. Res. Part I* **1993**, *40* (3), 629–641.

Bresnahan, P. J.; Martz, T. R.; Takeshita, Y.; Johnson, K. S.; LaShomb, M. Best Practices for Autonomous Measurement of Seawater PH with the Honeywell Durafet. *Methods Oceanogr.* **2014**, *9* (October), 44–60.

Broecker, W. S.; Takahashi, T.; Simpson, H. J.; Peng, T.-H. Fate of Fossil Fuel Carbon Dioxide and the Global Carbon Budget. *Science (80-.).* **1979**, *206* (4417), 409–418.

Byrne, R. H.; Mcelligott, S.; Feely, R. A.; Millero, F. J. The Role of PHP Measurements

in Marine CO -System Characterizations. *Deep. Res.* **1999**, *46*, 1985–1997.

Cai, W. J.; Hu, X.; Huang, W. J.; Jiang, L. Q.; Wang, Y.; Peng, T. H.; Zhang, X. Alkalinity Distribution in the Western North Atlantic Ocean Margins. *J. Geophys. Res. Ocean.* **2010**, *115* (8), 1–15.

Caldeira, K.; Wickett, M. E. Oceanography: Anthropogenic Carbon and Ocean PH. *Nature* **2003**, *425* (6956), 365.

De Carlo, E. H.; Beltran, V. L.; Tomlinson, M. S. Composition of Water and Suspended Sediment in Streams of Urbanized Subtropical Watersheds in Hawaii. *Appl. Geochemistry* **2004**, *19* (7), 1011–1037.

De Carlo, E. H.; Hoover, D. J.; Young, C. W.; Hoover, R. S.; Mackenzie, F. T. Impact of Storm Runoff from Tropical Watersheds on Coastal Water Quality and Productivity. *Appl. Geochemistry* **2007**, *22* (8 SPEC. ISS.), 1777–1797.

Clayton, T. D.; Byrne, R. H.; Breland, J. A.; Feely, R. A.; Millero, F. J.; Campbell, D. M.; Murphy, P. P.; Lamb, M. F. The Role of PH Measurements in Modern Oceanic CO2-System Characterizations: Precision and Thermodynamic Consistency. *Deep. Res. Part II* **1995**, *42* (2–3), 411–429.

Cullison Gray, S. E.; DeGrandpre, M. D.; Moore, T. S.; Martz, T. R.; Friederich, G. E.; Johnson, K. S. Applications of in Situ PH Measurements for Inorganic Carbon Calculations. *Mar. Chem.* **2011**, *125* (1–4), 82–90.

Cyronak, T.; Schulz, K. G.; Jokiel, P. L. The Omega Myth: What Really Drives Lower Calcification Rates in an Acidifying Ocean. *ICES J. Mar. Sci.* **2016**, *73* (3), 558–562.

Decarlo, T. M.; Cohen, A. L.; Wong, G. T. F.; Shiah, F.-K.; Lentz, S. J.; Davis, K. A.; Shamberger, K. E. F.; Lohmann, P. Community Production Modulates Coral Reef PH and the Sensitivity of Ecosystem Calcification to Ocean Acidification. *J. Geophys. Res.* **2017**, *122*, 745–761.

Decarlo, T. M.; Comeau, S.; Cornwall, C. E.; McCulloch, M. T. Coral Resistance to Ocean Acidification Linked to Increased Calcium at the Site of Calcification. *Proc. R. Soc. B Biol. Sci.* **2018**, *285* (1878).

Deffeyes, K. S. Carbonate Equilibria: A Graphic and Algebraic Approach. *Limnol. Oceanogr.* **1965**, *10* (3), 412–426.

DeGrandpre, M. D.; Hammar, T. R.; Smith, S. P.; Sayles, F. L. In Situ Measurements of Seawater PC0,. *Limnol. Oceanogr.* **1995**, *40* (5), 969–975.

DeGrandpre, M. D.; Martz, T. R.; Hart, R. D.; Elison, D. M.; Zhang, A.; Bahnson, A. G. Universal Tracer Monitored Titrations. *Anal. Chem.* **2011**, *83* (24), 9217–9220.

Dickson, A. G. An Exact Definition of Total Alkalinity and a Procedure for the Estimation of Alkalinity and Total Inorganic Carbon from Titration Data. *Deep Sea Res. Part I Oceanogr. Res. Pap.* **1981**, *28* (6), 609–623.

Dickson, A. G. The Development of the Alkalinity Concept in Marine Chemistry. *Mar. Chem.* **1992**, *40* (1–2), 49–63.

Dickson, A. G.; Millero, F. J. A Comparison of the Equilibrium Constants for the Dissociation of Carbonic Acid in Seawater Media. *Deep Sea Res. Part A, Oceanogr. Res. Pap.* **1987**, *34* (10), 1733–1743.

Dickson, A. G.; Sabine, C. L.; Christian, J. R. *Guide to Best Practices for Ocean CO 2 Measurements*; 2007.

DOE. Handbook of Methods for the Analysis of the Various Parameters of the Carbon

Dioxide System in Sea Water. *DOE Handb.* **1992**, *1994* (September), 22.

Doney, S. C.; Fabry, V. J.; Feely, R. a.; Kleypas, J. a. Ocean Acidification: The Other CO 2 Problem. *Ann. Rev. Mar. Sci.* **2009**, *1* (1), 169–192.

Dore, J. E.; Lukas, R.; Sadler, D. W.; Church, M. J.; Karl, D. M. Physical and Biogeochemical Modulation of Ocean Acidification in the Central North Pacific. *Proc. Natl. Acad. Sci. U. S. A.* **2009**, *106* (30), 12235–12240.

Drupp, P.; De Carlo, E. H.; Mackenzie, F. T.; Bienfang, P.; Sabine, C. L. Nutrient Inputs, Phytoplankton Response, and CO2 Variations in a Semi-Enclosed Subtropical Embayment, Kaneohe Bay, Hawaii. *Aquat. Geochemistry* **2011**, *17* (4–5), 473–498.

Drupp, P. S.; Carlo, E. H.; Mackenzie, F. T.; Sabine, C. L.; Feely, R. a.; Shamberger, K. E. Comparison of CO2 Dynamics and Air–Sea Gas Exchange in Differing Tropical Reef Environments. *Aquat. Geochemistry* **2013**.

Eyre, B. D.; Andersson, A. J.; Cyronak, T. Benthic Coral Reef Calcium Carbonate Dissolution in an Acidifying Ocean. *Nat. Clim. Chang.* **2014**, *4* (11), 969–976.

Fabry, V.; Seibel, B.; Feely, R.; Orr, J. Impacts of Ocean Acidification on Marine Fauna and Ecosystem Processes. *ICES J. Mar. Sci.* **2008**, *65* (Dic), 414–432.

Falter, J. L.; Atkinson, M. J.; Langdon, C. Production-Respiration Relationships at Different Timescales within the Biosphere 2 Coral Reef Biome. *Limnol. Oceanogr.* **2001**, *46* (7), 1653–1660.

Falter, J. L.; Atkinson, M. J.; Merrifield, M. a. Mass-Transfer Limitation of Nutrient Uptake by a Wave-Dominated Reef Flat Community. *Limnol. Oceanogr.* **2004**, *49* (5), 1820–1831.

Falter, J. L.; Lowe, R. J.; Atkinson, M. J.; Monismith, S. G.; Schar, D. W. Continuous Measurements of Net Production over a Shallow Reef Community Using a Modified Eulerian Approach. *J. Geophys. Res. Ocean.* **2008**, *113* (7), 1–14.

Falter, J. L.; Atkinson, M. J.; Schar, D. W.; Lowe, R. J.; Monismith, S. G. Short-Term Coherency between Gross Primary Production and Community Respiration in an Algal-Dominated Reef Flat. *Coral Reefs* **2011**, *30* (1), 53–58.

Falter, J. L.; Lowe, R. J.; Atkinson, M. J.; Cuet, P. Seasonal Coupling and De-Coupling of Net Calcification Rates from Coral Reef Metabolism and Carbonate Chemistry at Ningaloo Reef, Western Australia. *J. Geophys. Res. Ocean.* **2012**, *117* (5), 1–14.

Falter, J. L.; Lowe, R. J.; Zhang, Z.; McCulloch, M. Physical and Biological Controls on the Carbonate Chemistry of Coral Reef Waters: Effects of Metabolism, Wave Forcing, Sea Level, and Geomorphology. *PLoS One* **2013**, *8* (1), e53303.

Gattuso, J.-P.; Pichon, M.; Delesalle, B.; Canon, C.; Frankignoulle, M. Carbon Fluxes in Coral Reefs . I . Lagrangian Measurement of Community Metabolism and Resulting Air-Sea CO2 Disequilibrium. *Mar. Ecol. Prog. Ser.* **1996**, *145*, 109–121.

Gattuso, J.-P.; Frankignoulle, M.; Wollast, R. Carbon and Carbonate Metabolism in Coastal Aquatic Ecosystems. *Annu. Rev. Ecol. Syst.* **1998**, *29* (1), 405–434.

Gattuso, J.-P.; Allemand, D.; Frankignoulle, M. Photosynthesis and Calcification at Cellular , Organismal and Community Levels in Coral Reefs : A Review on Interactions and Control by Carbonate. *Amer. Zool* **1999**, *39*, 160–183.

Gray, S.; Ellis, P.; Grace, M.; Mckelvie, I. Underway Determination of Alkalinity in

Estuarine Waters by Reagent-Injection Gas-Diffusion Flow Analysis. *Talanta* **2008**, *77* (2), 533–540.

Gray, S. E. C.; Degrandpre, M. D.; Langdon, C.; Corredor, J. E. Short-Term and Seasonal PH. *Global Biogeochem. Cycles* **2012**, *26* (3), GB3012.

Hansson, I.; Jagner, D. Evaluation of the Acuracy of Gran Plots by Means of Computer Calculations. Application to the Potentiometric Titration of the Total Alkalinity and Carbonate Content of Sea Water. *Anal. Chim. Acta* **1973**, *65*, 363–373.

Ho, D. T.; Law, C. S.; Smith, M. J.; Schlosser, P.; Harvey, M.; Hill, P. Measurements of Air-Sea Gas Exchange at High Wind Speeds in the Southern Ocean: Implications for Global Parameterizations. *Geophys. Res. Lett.* **2006**, *33* (16), L16611.

Hofmann, G. E.; Barry, J. P.; Edmunds, P. J.; Gates, R. D.; Hutchins, D. A.; Klinger, T.; Sewell, M. A. The Effect of Ocean Acidification on Calcifying Organisms in Marine Ecosystems: An Organism-to-Ecosystem Perspective. *Annu. Rev. Ecol. Evol. Syst. Vol 41* **2010**, *41* (July), 127–147.

Hofmann, G. E.; Smith, J. E.; Johnson, K. S.; Send, U.; Levin, L. A.; Micheli, F.; Paytan, A.; Price, N. N.; Peterson, B.; Takeshita, Y.; et al. High-Frequency Dynamics of Ocean PH: A Multi-Ecosystem Comparison. *PLoS One* **2011**, *6* (12), e28983.

Hönisch, B.; Ridgwell, A.; Schmidt, D. N.; Thomas, E.; Gibbs, S. J.; Sluijs, A.; Zeebe, R.; Kump, L.; Martindale, R. C.; Greene, S. E.; et al. The Geological Record of Ocean Acidification. *Science* **2012**, *335* (6072), 1058–1063.

Hoover, D. J.; MacKenzie, F. T. Fluvial Fluxes of Water, Suspended Particulate Matter, and Nutrients and Potential Impacts on Tropical Coastal Water Biogeochemistry: Oahu, Hawai'i. *Aquat. Geochemistry* **2009**, *15* (4), 547–570.

Johnson, K. M.; Sieburth, J. M. Coulometric Total Carbon Dioxide Analysis for Marine Studies: Automation and Calibration. *Mar. Chem.* **1987**, *21*, 117–133.

Jury, C. P.; Whitehead, R. F.; Szmant, A. M. Effects of Variations in Carbonate Chemistry on the Calcification Rates of Madracis Auretenra (= Madracis Mirabilis Sensu Wells, 1973): Bicarbonate Concentrations Best Predict Calcification Rates. *Glob. Chang. Biol.* **2010**, *16* (5), 1632–1644.

Kinsey, D. W. Metabolism, Calcification and Carbon Production: 1 Systems Level Studies. *The Fifth International Coral Reef Congress*. 1985, pp 505–526.

Kleypas, J. A.; Feely, R. A.; Fabry, V. J.; Langdon, C.; Sabine, C. L.; Robbins, L. L.; Allemand, D.; Balch, W. M.; Berelson, W. M.; Gattuso, J. P.; et al. Impacts of Ocean Acidification on Coral Reefs and Other Marine Calcifiers: A Guide for Future Research. *A Rep. a Work. held 18–20 April 2005, St. Petersburg, FL, Spons. by NSF, NOAA, U.S. Geol. Surv.* **2006**, 88 pages.

Kortzinger, A.; Mintrop, L.; Wallace, D. W. R.; Johnson, K. M.; Neill, C.; Tilbrook, B.; Towler, P.; Inoue, H. Y.; Ishii, M.; Shaffer, G.; et al. Körtzinger et Al. - 2000 - The International at-Sea Intercomparison of FCO2 Systems during the RV Meteor Cruise 361 in the North Atlanti.Pdf. **2000**, 171–192.

Langdon, C.; Takahashi, T.; Marubini, F.; Atkinson, M.; Sweeney, C.; Aceves, H.; Barnett, H.; Chipman, D.; Goddard, J. Effect of Calcium Carbonate Saturation State on the Rate of Calcification of an Experimental Coral Reef. *Global Biogeochem. Cycles* **2000**, *14(2)* (10.1594/PANGAEA.721195), 639–654.

Lantz, C. a.; Atkinson, M. J.; Winn, C. W.; Kahng, S. E. Dissolved Inorganic Carbon and Total Alkalinity of a Hawaiian Fringing Reef: Chemical Techniques for

Monitoring the Effects of Ocean Acidification on Coral Reefs. *Coral Reefs* **2013**.

Lee, K.; Millero, F. J. Thermodynamic Studies of the Carbonate System in Seawater. *Deep. Res. Part I* **1995**, *42* (11–12), 2035–2061.

Lee, K.; Millero, F. J.; Byrne, H.; Feely, A.; Wanninkhof, R. The Recommended Dissociation Constants for Carbonic Acid in Seawater. *Geophys. Res. Lett.* **2000**, *27* (2), 229–232.

Lewis, E.; Wallace, D. Program Developed for CO2 System Calculations. *Ornl/Cdiac-105* **1998**, 1–21.

Li, Q.; Wang, F.; Wang, Z. A.; Yuan, D.; Dai, M.; Chen, J.; Dai, J.; Hoering, K. a. Automated Spectrophotometric Analyzer for Rapid Single-Point Titration of Seawater Total Alkalinity. *Environ. Sci. Technol.* **2013**, *47* (19), 11139–11146.

Lowe, R. J.; Falter, J. L.; Monismith, S. G.; Atkinson, M. J. A Numerical Study of Circulation in a Coastal Reef-Lagoon System. *J. Geophys. Res. Ocean.* **2009a**, *114* (6), 1–18.

Lowe, R. J.; Falter, J. L.; Monismith, S. G.; Atkinson, M. J. Wave-Driven Circulation of a Coastal Reef–Lagoon System. *J. Phys. Oceanogr.* **2009b**, *39* (4), 873–893.

Martz, T. R.; Carr, J. J.; French, C. R.; DeGrandpre, M. D. A Submersible Autonomous Sensor for Spectrophotometric PH Measurements of Natural Waters. *Anal. Chem.* **2003**, *75* (8), 1844–1850.

Martz, T. R.; Dickson, A. G.; DeGrandpre, M. D. Tracer Monitored Titrations: Measurement of Total Alkalinity. *Anal. Chem.* **2006**, *78* (6), 1817–1826.

Martz, T. R.; Connery, J. G.; Johnson, K. S. Testing the Honeywell Durafet for Seawater PH Applications. *Limnol. Oceanogr. Methods* **2010**, *8*, 172–184.

Massaro, R. F. S.; Carlo, E. H.; Drupp, P. S.; Mackenzie, F. T.; Jones, S. M.; Shamberger, K. E.; Sabine, C. L.; Feely, R. A. Multiple Factors Driving Variability of CO2 Exchange Between the Ocean and Atmosphere in a Tropical Coral Reef Environment. *Aquat. Geochemistry* **2012**, *18* (4), 357–386.

McCulloch, M.; Falter, J.; Trotter, J.; Montagna, P. Coral Resilience to Ocean Acidification and Global Warming through PH Up-Regulation. *Nat. Clim. Chang.* **2012**, *2* (8), 623–627.

McElligott, S.; Byrne, R. H.; Lee, K.; Wanninkhof, R.; Millero, F. J.; Feely, R. A. Discrete Water Column Measurements of CO2 Fugacity and PH(T) in Seawater: A Comparison of Direct Measurements and Thermodynamic Calculations. *Mar. Chem.* **1998**, *60* (1–2), 63–73.

McMahon, A.; Santos, I. R.; Cyronak, T.; Eyre, B. D. Hysteresis between Coral Reef Calcification and the Seawater Aragonite Saturation State. *Geophys. Res. Lett.* **2013**, *40* (July), n/a-n/a.

McMahon, A.; Santos, I. R.; Schulz, K. G.; Cyronak, T.; Maher, D. T. Determining Coral Reef Calcification and Primary Production Using Automated Alkalinity, PH and p CO 2 Measurements at High Temporal Resolution. *Estuar. Coast. Shelf Sci.* **2018**.

Mehrbach, C.; Culberson, C. H.; Hawley, J. E.; Pytkowicz, R. M. Measurement of the Apparent Dissociation Constants of Carbonic Acid in Seawater at Atmospheric Pressure. *Limnol. Oceanogr.* **1973**, *18* (6), 897–907.

Millero, F. The Marine Inorganic Carbon Cycle. *Chem. Rev.* **2007**, *107* (Table 1), 308–341.

Ohde, S.; Woesik, R. V. Carbon Dioxide Flux and Metabolic Processes of a Coral Reef ,

Okinawa Shigeru Ohde and Robert van Woesik. *Bull Mar Sci* **1999**, *65* (2), 559–576.

Orr, J. C.; Fabry, V. J.; Aumont, O.; Bopp, L.; Doney, S. C.; Feely, R. A.; Gnanadesikan, A.; Gruber, N.; Ishida, A.; Joos, F.; et al. Anthropogenic Ocean Acidification over the Twenty-First Century and Its Impact on Calcifying Organisms. *Nature* **2005**, *437* (7059), 681–686.

Raven, J. A.; Elderfield, H.; Hoegh-Guldberg, O.; Liss, P.; Riebesell, U.; Shepherd, J.; Turley, C.; Watson, A. Ocean Acidification Due to Increasing Atmospheric Carbon Dioxide. *R. Soc.* **2005**, No. June, 68.

Ringuet, S.; Mackenzie, F. T. Controls on Nutrient and Phytoplankton Dynamics during Normal Flow and Storm Runoff Conditions, Southern Kaneohe Bay, Hawaii. *Estuaries* **2005**, *28* (3), 327–337.

Roleda, M. Y.; Boyd, P. W.; Hurd, C. L. Before Ocean Acidification: Calcifier Chemistry Lessons. *J. Phycol.* **2012**, *48* (4), 840–843.

Sabine, C. L.; Feely, R. a; Gruber, N.; Key, R. M.; Lee, K.; Bullister, J. L.; Wanninkhof, R.; Wong, C. S.; Wallace, D. W. R.; Tilbrook, B.; et al. The Oceanic Sink for Anthropogenic CO2. *Science* **2004**, *305* (5682), 367–371.

Sayles, F. L.; Eck, C. An Autonomous Instrument for Time Series Analysis of TCO2 from Oceanographic Moorings. *Deep Sea Res. Part I Oceanogr. Res. Pap.* **2009**, *56* (9), 1590–1603.

Schneider, B.; Sadkowiak, B.; Wachholz, F. A New Method for Continuous Measurements of O2 in Surface Water in Combination with PCO2 Measurements: Implications for Gas Phase Equilibration. *Mar. Chem.* **2007**, *103* (1–2), 163–171.

Seidel, M. P.; DeGrandpre, M. D.; Dickson, A. G. A Sensor for in Situ Indicator-Based Measurements of Seawater PH. *Mar. Chem.* **2008**, *109* (1–2), 18–28.

Shamberger, K. E. F.; Feely, R. a.; Sabine, C. L.; Atkinson, M. J.; DeCarlo, E. H.; Mackenzie, F. T.; Drupp, P. S.; Butterfield, D. a. Calcification and Organic Production on a Hawaiian Coral Reef. *Mar. Chem.* **2011**, *127* (1–4), 64–75.

Shaw, E. C.; McNeil, B. I.; Tilbrook, B. Impacts of Ocean Acidification in Naturally Variable Coral Reef Flat Ecosystems. *J. Geophys. Res. Ocean.* **2012**, *117* (3), 1–14.

Shaw, E. C.; Phinn, S. R.; Tilbrook, B.; Steven, A. Natural in Situ Relationships Suggest Coral Reef Calcium Carbonate Production Will Decline with Ocean Acidification. *Limnol. Oceanogr.* **2015**.

Silverman, J.; Lazar, B.; Erez, J. Effect of Aragonite Saturation, Temperature, and Nutrients on the Community Calcification Rate of a Coral Reef. *J. Geophys. Res.* **2007**, *112* (C5), C05004.

Silverman, J.; Kline, D. I.; Johnson, L.; Rivlin, T.; Schneider, K.; Erez, J.; Lazar, B.; Caldeira, K. Carbon Turnover Rates in the One Tree Island Reef: A 40-Year Perspective. *J. Geophys. Res.* **2012**, *117* (G3), G03023.

Smith, S. V.; Key, G. S. Carbon Dioxide and Metabolism in Marine Environments. *Limnol. Oceanogr.* **1975**, *20* (3), 493–495.

Smith, S. V; Kimmerer, W. J.; Laws, E. A.; Brock, R. E.; Walsh, T. W. Kaneohe Bay Sewage Diversion Experiment: Perspectives on Ecosystem Responses to Nutritional Perturbation. *Pacific Sci.* **1981**, *35* (4), 279–395.

Spaulding, R. S.; DeGrandpre, M. D.; Beck, J. C.; Hart, R. D.; Peterson, B.; De Carlo, E.

H.; Drupp, P. S.; Hammar, T. R. Autonomous in Situ Measurements of Seawater Alkalinity. *Environ. Sci. Technol.* **2014**, *48* (16), 9573–9581.

Sutton, A. J.; Feely, R. A.; Sabine, C. L.; McPhaden, M. J.; Takahashi, T.; Chav. Natural Variability and Anthropogenic Change in Equatorial Pacific Surface Ocean PCO2 and PH. *Global Biogeochem. Cycles* **2014**, *28*, 131–145.

Sutton, A. J.; Sabine, C. L.; Maenner-Jones, S.; Lawrence-Slavas, N.; Meinig, C.; Feely, R. A.; Mathis, J. T.; Musielewicz, S.; Bott, R.; McLain, P. D.; et al. CDIAC Data Management and Archival Support for a High-Frequency Atmospheric and Seawater PCO 2 Data Set from 14 Open Ocean Moorings. *Earth Syst. Sci. Data* **2015**, *17* (January), 6864.

Sutton, A. J.; Feely, R. A.; Maenner-jones, S.; Musielwicz, S.; Osborne, J.; Monacci, N.; Cross, J.; Bott, R.; Kozyr, A. Autonomous Seawater PCO2 and PH Time Series from 40 Surface Buoys and the Emergence of Anthropogenic Trends. *Earth Syst. Sci. Data* **2018**, *1* (August), 1–23.

Suzuki, A.; Kawahata, H. Carbon Budget of Coral Reef Systems: An Overview of Observations in Fringing Reefs, Barrier Reefs and Atolls in the Indo-Pacific Regions. *Tellus B* **2003**, *55* (2), 428–444.

Takahashi, T.; Sutherland, S. C.; Wanninkhof, R.; Sweeney, C.; Feely, R. A.; Chipman, D. W.; Hales, B.; Friederich, G.; Chavez, F.; Sabine, C.; et al. Climatological Mean and Decadal Change in Surface Ocean PCO2, and Net Sea-Air CO2flux over the Global Oceans. *Deep. Res. Part II Top. Stud. Oceanogr.* **2009**, *56* (8–10), 554–577.

Takeshita, Y.; Mcgillis, W.; Briggs, E. M.; Carter, A. L.; Donham, E. M.; Martz, T. R.; Price, N. N.; Smith, J. E. Journal of Geophysical Research : Oceans Coral Reef Using a Boundary Layer Approach. *J. Geophys. Res. Ocean.* **2016**, 5655–5671.

Venti, a.; Andersson, a.; Langdon, C. Multiple Driving Factors Explain Spatial and Temporal Variability in Coral Calcification Rates on the Bermuda Platform. *Coral Reefs* **2014**, 979–997.

Watanabe, A.; Kayanne, H.; Nozaki, K.; Kato, K.; Negishi, A.; Kudo, S.; Kimoto, H.; Tsuda, M.; Dickson, A. G. A Rapid, Precise Potentiometric Determination of Total Alkalinity in Seawater by a Newly Developed Flow-through Analyzer Designed for Coastal Regions. *Mar. Chem.* **2004**, *85* (1–2), 75–87.

Weiss, R. F. Carbon Dioxide in Water and Seawater: The Solubility of a Non-Ideal Gas. *Mar. Chem.* **1974**, *2* (3), 203–215.

Yao, W.; Byrne, R. H. Simplified Seawater Alkalinity Analysis: Use of Linear Array Spectrometers. *Deep. Res. Part I Oceanogr. Res. Pap.* **1998**, *45* (8), 1383–1392.